AN ABSTRACT OF THESIS OF

Minkmas Vatanatham for the degree of Master of Science in Chemical Engineering presented on August 3, 2000. Title: Surface Nucleation of Hydroxyapatite onto Titanium Substrates Thermally Treated with Oxygen.

Abstract approved: Redacted for Privacy

Shoichi Kimura

Hydroxyapatite (HAP), $Ca_{10}(PO_4)_6(OH)_2$ with Ca/P ratio of 1.67, has been used widely in the medical field due to its excellent bioactivity. However, its mechanical properties are very poor, which limits its application as a bone implant material. This problem can possibly be solved by coating HAP on titanium substrates to manufacture coated implants with the ductility of the underlying metal and the bioactivity of the surface. An easy and new method of thermal oxidation at relatively low temperature was proposed in this research to modify the surface of Ti substrates to titanium dioxide with both rutile and anatase phases for enhancing HAP surface nucleation. HAP was then successfully coated on titanium substrates after oxidation in oxygen at 610 °C for 1 hour, and aging in a supersaturated solution of 1.20 mM PO_4^{3-} and 2.00 mM Ca^{2+} (starting Ca/P ratio = 1.67). After aging for 2 days, XPS analysis showed Ti, Ca, and P surface concentrations of 0.0%, 17.8%, and 10.7% respectively, with a Ca/P ratio of 1.62. The total coverage of HAP on the oxide layer was demonstrated by a Ti surface concentration of zero. After aging for 10 days, the surface concentration of Ca went up to 21.1% and that of P went up to 12.7% with a

Ca/P ratio of 1.66. The corresponding SEM image shows HAP coverage on the surface as rose-like structures.

XRD patterns of simultaneously crystallized powder from the solution were very well matched with that of the reference HAP. There was no HAP detected on the surface of titanium oxidized in air at temperatures ranging from 600 to 900 °C. The presence of both anatase and rutile TiO_2 after thermal oxidation in O_2 at low temperature was believed to enhance the HAP surface nucleation. It is expected that this method can be used to form a dense layer of HAP with total coverage on titanium substrates in a room temperature process during all steps involving HAP, in order to eliminate the phase decomposition. It is an easy method to reproduce with low operating and equipment costs, and high accommodativeness for coating HAP on any shape of Ti implant material.

Surface Nucleation of Hydroxyapatite onto Titanium Substrates Thermally Treated with Oxygen.

by

Minkmas Vatanatham

A Thesis Submitted
to
Oregon State University

In Partial Fulfillment of
the requirements for the degree of

Master of Science

Presented August 3, 2000
Commencement June 2001

Master of Science thesis of Minkmas Vatanatham presented on August 3, 2000.

APPROVED:

Redacted for Privacy

Major Professor, representing Chemical Engineering

Redacted for Privacy

Chair of Department of Chemical Engineering

Redacted for Privacy

Dean of the Graduate School

I understand that my thesis will become part of the permanent collection of Oregon State University libraries. My signature below authorizes release of my thesis to any reader upon request.

Redacted for Privacy

Minkmas Vatanatham, Author

ACKNOWLEDGEMENT

I would like to show my sincere appreciation to people as follows:

- Dr. Shoichi Kimura, my advisor, for his time, comments, and supports
- My father, my mother, my sister, and my friends, for all the friendship we have had
- My committee members: Dr. Jennifer Field, Dr. John Wager, and Dr. Chih-hung Chang, for their time and suggestions
- Mr. Dale Govier, from the Department of Energy in the Albany Research Center, for allowing and teaching me to use the XPS machine
- All faculty and staff in the Department of Chemical Engineering, for providing me knowledge and being helpful during my 2 years at Oregon State University
- And Barry Williams, for staying up late with me in those long nights.

TABLE OF CONTENTS

TABLE OF CONTENTS (Continued)

LIST OF FIGURES

LIST OF TABLES

LIST OF APPENDIX FIGURES

LIST OF APPENDIX FIGURES (CONTINUED)

Surface Nucleation of Hydroxyapatite onto Titanium Substrates Thermally Treated with Oxygen.

CHAPTER 1

BACKGROUND, JOURNAL REVIEW, AND OBJECTIVES

BACKGROUND

Several choices of material are available for use as implant material, including alumina (Hata et al., 1995), collagen membrane (Rhee, 1998), polymers (Daw et al., 1998), silica glass (Abe et al., 1990), tantalum (Wen et al., 1998), titanium (Wei, et al. 1999), and titanium-vanadium alloy, i.e. Ti-6Al-4V, (Kurzweg et al., 1998). Titanium has a high strength-to-weight ratio, low elastic modulus, excellent corrosion resistance from protective superficial TiO_2 films (2-3 nm thick), and has hypoallergenic qualities. From all these beneficial properties, titanium has been used increasingly as an implant material in pacemaker casings, orthopedic devices, and dental applications. However, the biocompatibility of titanium, a very important required property for bone implant materials, is very poor.

Hydroxyapatite ($Ca_{10}(PO_4)_6(OH)_2$) or HAP is a class of calcium phosphate-based materials and has been used in various forms in the medical field due to its presence as bone apatite, or the calcium phosphate mineral present in biological hard tissue. This results in its excellent bioactivity, or capability to bind with living tissue. HAP constitutes approximately 70% (by weight) of natural bone while the rest is

organic, largely collagen (Rhee, 1998). Being osteoconductive (defined as the ability for osteoblasts, or bone forming cells in blood plasma, to proliferate), one of its applications is to serve as an interfacial bioactive phase between the implant and surrounding tissue after implantation (Wang et al., 1999). Owing to the chemical similarity of HAP to the inorganic component of the composite material in bone, its presence at the implant surface helps to develop a tight bond between implant material and living bone. It is thus able to improve fixation and stability of the implant, and thus decrease recovery time after implantation (Kurzweg et al., 1998). However, HAP has some disadvantages, such as its brittleness, low tensile strength, and low fracture toughness. In fact, the brittleness is a serious obstacle to the application of HAP as load-bearing implants (Nonami et al., 1998).

A possible solution is to combine the excellent bioactivity of HAP and the excellent mechanical properties of titanium. Attention has therefore been focused on the formation of HAP coatings on titanium by several methods. The coated implant will have the ductility of the underlying metal, as well as a bioactive surface. There are a number of additional benefits with this coating, including faster adaptation of the implant to surrounding tissue with reduced healing time, enhancement of bone formation, firmer implant-bone attachment, and the reduction of metallic ion release (Han et al., 1999).

Performance of such coatings depends on a large array of factors, most notably coating thickness, total coverage, homogeneity, crystallinity, phase purity, adhesive strength, accommodativeness to coat any shape, fast nucleation rate, and

resorption resistance. In addition to bioactivity, an HAP coating satisfactory for clinical use must be porous, hard, tough, and adherent.

Sahay et al. (1994) reported required characteristics of composite HAP coatings for medical and dental devices. It was stated that a 40-450 μm pore size range is optimistic for bony ingrowth. Depending on the specific requirements, orthopedic implants (knee, hip joint, shoulder joint, etc.) and other medical devices can have a thin layer or multilayer metallic porous structure in the thickness range of 0.25-1.5 mm. The thickness of the HAP outer layer remains approximately 25 μm as in dental coatings. The average tensile and shear strengths of the orthopedic coating are 35.8 MPa and 15.1 MPa respectively, whereas those for the dental composite coating are 38.6 MPa and 22.7 MPa, respectively.

People have tried many methods in order to meet the goal of a thick porous HAP layer, with high purity, high crystallinity, high tensile and shear strength, high accommodativeness to coat any shape, and fast nucleation rate. The following are some methods that have been studied widely.

JOURNAL REVIEW

Electrophotoretic deposition

In this process, charged ceramic particles suspended in solution are uniformly deposited on the metal substrate by electrophoresis. This is a low-cost flexible coating process, and being a non-line-of-sight coating process, it can be used to deposit

uniform coatings on substrates of complex shape or surface morphology. However, the electrophotoretic-coated implants need a subsequent densification stage in order to sinter the coating. This requirement poses something of a dilemma. If the thermal expansion coefficient of the ceramic coating is lower than the substrate, then the coating is placed in compression on cooling, and if higher, then the coating is placed in tension on cooling. Ideally, the thermal expansion coefficient of the coating and substrate should be very similar. The thermal expansion coefficient of titanium is 10.4 $\mu m \cdot (mK)^{-1}$ while that of metathesis HAP is 13.4 $\mu m \cdot (mK)^{-1}$. This will lead to cracking at higher temperature due to shrinkage. It was found that after heating to 1000 °C, the shrinkage was 17.87% (Wei et al., 1999). Furthermore, low sintering temperatures can lead to weakly bonded low-density coating. It is seen that the cracking problem still can not be solved.

Plasma spraying

In this technique, HAP powder is sprayed onto substrate plates to form a bioactive coating by using a high voltage plasma spray system. Argon is used as the main plasma forming gas and helium as the auxiliary gas with a pressure of 0.28 MPa for each gas. This process could quickly form a monolayer of HAP as thick as 400 μm (Wang et al., 1999). This has been the most commonly used method in the past decade to obtain coatings for implant fixation, even though many of the same concerns remain, including relatively poor substrate-coating bond strengths that can result in long term service failure (Filiaggi et al., 1996). In addition, studies have

shown that HAP coatings formed by plasma spraying are especially structurally, and possibly chemically, inhomogeneous, resulting in regions prone to uncontrolled dissolution and subsequent coating degradation or delamination over time. This technique has a very high operating cost and presents difficulty in producing a porous coating.

Porous coatings can greatly enhance the establishment of strong bonding between implants and bone (Weng, 1998). The temperature during plasma spraying can be as high as 10,000-30,000 °C. It has been reported that HAP easily decomposes at high temperatures, and that HAP peels off after long-term use in a body (Han et al., 1999). The high temperatures in plasma jets inevitably leads to changes in the degree of crystallinity, i.e. development of amorphous calcium phosphate, and in the phase composition by partial dehydration of HAP to oxyhydroxyapatite or oxyapatite and thermal transformation of HAP into tri- or tetracalcium phosphate or even non-biocompatible CaO. Because these phases seem to decrease the adhesion strength to the metallic substrate, and have a lower resorption resistance than does stoichiometric HAP, their occurrence must be suppressed (Kurzweg et al., 1998). Ellies et al. (1992) showed that degradation of HAP in plasma-sprayed coating is severe if the starting powder is calcium-deficient HAP ($1.33 < Ca/P < 1.67$). Thus it is necessary to explore the technique of coating HAP at low temperature.

Solid-gel thin film

Sol-gel thin film processing by an alkoxide route represents an alternative approach for obtaining thin ceramic coatings over metal substrates. It is also called a dip coating-sintering method, wherein metal and ceramic substrates are dipped into a slurry containing HAP powder, then sintered at an appropriate time-temperature cycle to densify the ceramic coating. This technique offers a number of advantages over other coating methods, including precise microstructural and chemical control and the ability to produce new amorphous and crystalline ceramics. Ease of processing with minimal capital or equipment cost makes the process especially attractive on an industrial/commercial scale (Filiaggi et al., 1996). However, similar to the electrophotoretic deposition method, this method needs a subsequent densification stage at temperatures in the range of 500-1000 °C in order to sinter the coating. Higher temperatures will lead to higher crystallinity and higher shear strength but with a higher tendency for decomposition. Even though the sintering was done for as long as 12-24 hours per cycle, the adhesive force was still low, 10-12 MPa, in the 500-750 °C temperature range (Weng, 1998). Another problem with this method is that one process cycle gives a very small thickness (nanometers) which makes the process more complicated to achieve the desired thickness and porosity.

Simulated body fluid

This is a biomimetic process involving soaking substrates in a simulated body fluid in contact with a bioactive glass (Glass G). According to Abe et al. (1990), a

simulated body fluid has ion concentrations close to those of human blood plasma and is prepared from dissolving NaCl, $NaHCO_3$, KCl, $K_2HPO_4 \cdot 3H_2O$, $MgCl_2 \cdot 6H_2O$, $CaCl_2$, and Na_2SO_4 in deionized water which is buffered at pH 7.25. The ion concentration of simulated body fluid is 142 mM Na^+, 5 mM K^+, 2.5 mM Ca^{2+}, 148.8 mM Cl^-, 1 mM HPO_4^{2-}, and 0.5 mM SO_4^{2-}. Glass G was prepared by pouring a melt of nominal composition (in wt.%) MgO 4.6, CaO 44.7, SiO_2 34.0, P_2O_3 16.2 and CaF_2 0.5 onto a stainless steel plate, followed by a pressing with another stainless steel plate for a glass plate thickness of 2 mm. Just after being pressed, the resulting glass plate was held at 700 °C for 2 hours in a furnace to remove strains. This method is expected to yield a dense and uniform (continuous and homogeneous) layer of a bone-like apatite, which can be formed on various substrates including ceramics, metals, and organic polymers. The thickness varies from 1 μm to 15 μm after 7 days depending on the concentration of the solution.

This method does not require any subsequent high temperature sintering, but it does not yield high enough adhesive strengths between the apatite layer and the substrate; ranging from 9.8-11.5 MPa (Kokubo et al., 1996). This process is very hard to reproduce due to the many components present in solution, each of which requiring precise concentration control over several days for uniform layer growth. In addition, it has not been proven that this method can form a thick HAP coating.

Self-assembled monolayer

Self-assembled monolayers provide a molecular template to control the nucleation and growth of ceramic thin films. Self-assembly techniques from dilute solutions have been used for several years to prepare a custom-designed surface with well-defined chemical and physical properties. Strong chemical interactions between the adsorbate and substrate, and lateral interactions between the aliphatic components of the adsorbate result in the spontaneous assembly of films that can be highly crystalline and stable (King et al., 1990). A few groups of people have tried this method for the particular application of ceramic coatings on metal surfaces for bone implants. Mao et al. (1998) prepared the functionalized titanium surface through initial hydroxylation with H_2O_2 and subsequent self-assembly of vinyltriethoxysilane for 2 weeks, followed by oxidation of vinyl groups with dilute $KMnO_4$ solution into alcoholic hydroxyl groups and then into carboxyl groups. Treated plates were then immersed in supersaturated HAP solution for up to 2 months. An HAP layer of thicker than 40 μm had been formed. Campbell et al. (1996) formed a self-assembled monolayer on Ti-6Al-4V surface by placing the wafers in a 1% silane:cyclohexane solution for 30 minutes. The terminus vinyl group of the alkylsilane tether was subsequently modified to sulfonic acid by exposure of the derivatized wafer to SO_3 gas in a reaction vessel for 1 minute. The treated surface was then placed in supersaturated solutions of phosphate and calcium ions to form HAP. No thickness was reported in this work. The self-assembled monolayer method is a room temperature process that does not require subsequence sintering. However, the

nucleation rate is too slow and there is no proof of uniformity and purity of the HAP layer.

None of these methods have met the requirements of HAP coatings for bone implant material: thick, porous, strongly bound to Ti substrate, and accommodating to any shape. In addition, all steps involving HAP must be at a low temperature to minimize phase decomposition. It may be difficult to form a porous layer as thick as 1 mm (to sustain stable >40 μm pores of HAP); it cannot be done in only one process. From all methods people have tried, if the layer is thick and porous, it might have a problem with shear strength, while some methods that give high shear strength cannot form a thick and porous layer. This research proposes a novel idea for HAP coating on a titanium substrate for bone implant material. It would be more possible to strengthen the thick layer of HAP by first covering the total surface of titanium with a layer of dense, uniform HAP, then depositing porous thick layers on top with the help of molecular recognition. However, the purity, total coverage, low temperature procedures for all steps involving HAP, accommodativeness to coat any shape, and ease of method are very important factors for this first layer. All steps involving HAP should be done at room temperature to eliminate the possibility of decomposition to other forms of calcium phosphate.

Soten et al. (1999) grew a multilayer composite calcium dodecylphosphate-HAP-TiO_2-Ti in which the calcium dodecylphosphate was both stereochemically- and charge-matched with the HAP. Before immersion in supersaturated solution in the HAP coating step on the Ti substrate, TiO_2, believed to help HAP nucleating on surface, was sputter-deposited on Ti. TiO_2 was produced using a titanium target and a

mixed argon-oxygen atmosphere. Sputtering was performed for different periods of time at 1000 V dc at 12 mTorr pressure with 6 sccm argon and 6 sccm oxygen. By adjusting the sputtering conditions, the deposited film could be arrranged to be crystalline rutile and/or anatase or amorphous titania. A dense layer of HAP a few microns thick was then formed in a supersaturated solution of calcium and phosphate in 3 days.

However, this method requires a very expensive apparatus. It is also not a proper method for depositing a uniform layer of HAP on complex shapes, which is a big limitation for bone implant material application.

It is necessary to develop an easy, economical method for preparing a proper surface oxide to replace sputtering. This research looks into the possibility of using thermal oxidation to prepare a TiO_2 mixture of rutile and anatase phases to enhance HAP surface nucleation, which is very easy to operate, is expected to be reproducible, and accommodates any shape of implant material.

OBJECTIVES

The objective of this research is to form the first dense layer of HAP with total coverage on titanium substrates, in a process at room temperature during all steps involving HAP formation to eliminate phase decomposition. The surface is prepared by thermal oxidation at a proper condition to form a rutile and anatase mixture of TiO_2, then immersed in a supersaturated solution containing calcium and phosphate for HAP surface nucleation. Two oxidation surfaces are compared: oxidation in an O_2

stream and oxidation in an air stream. It will provide an easy method with low operating and equipment cost, and high accommodativeness to coat HAP on any shape of Ti implant material.

CHAPTER 2

MATERIALS AND METHODS

Crystallization of HAP can be written in terms of equation (1).

$$10Ca^{2+} + 6PO_4^{3-} + 2OH^- = Ca_{10}(PO_4)_6(OH)_2 \quad (1)$$

Calcium ions can come from $Ca(OH)_2$, $Ca(NO_3)_2$, or $CaCl_2$, while phosphate ions can come from Na_2HPO_4, $(NH_4)_2HPO_4$, H_3PO_4, or KH_2PO_4. $CaCl_2$ and KH_2PO_4 were chosen for this work because previous literature has reported their use in supersaturated solutions for HAP surface nucleation (Campbell et al., 1996; Soten et al., 1999).

In a calcium and phosphate aqueous system, many forms of calcium phosphate can crystallize. Table 1 shows all major calcium phosphates that might be in equilibrium in a calcium and phosphate aqueous system. It also shows a stoichiometric Ca/P ratio that increases from 1.00 of monetite to 1.67 of HAP.

Table 1. Calcium phosphates in a calcium and phosphate aqueous system.

Calcium phosphates	Formula	Ca/P
Monetite (shown as DCPA in Figure 1)	$CaHPO_4$	1.00
Dicalcium phosphate dihydrate, DCPD	$CaHPO_4 \cdot 2H_2O$	1.00
Octacalcium phosphate, OCP	$Ca_8H_2(PO_4)_6 \cdot 5H_2O$	1.33
β-Tricalcium phosphate, TCP	$Ca_3(PO_4)_2$	1.50
Hydroxyapatite, HAP	$Ca_5(PO_4)_3(OH)_2$	1.67

Solubility isotherms for data at 25 °C of several calcium phosphates in ternary systems are shown in Figure 1 (Gregory et al., 1974). TCP is second only to HAP in stability at pH above 6.36. The calculated pH of the singular points at 25 °C for TCP with DCPD and monetite are 5.88 and 6.36, respectively.

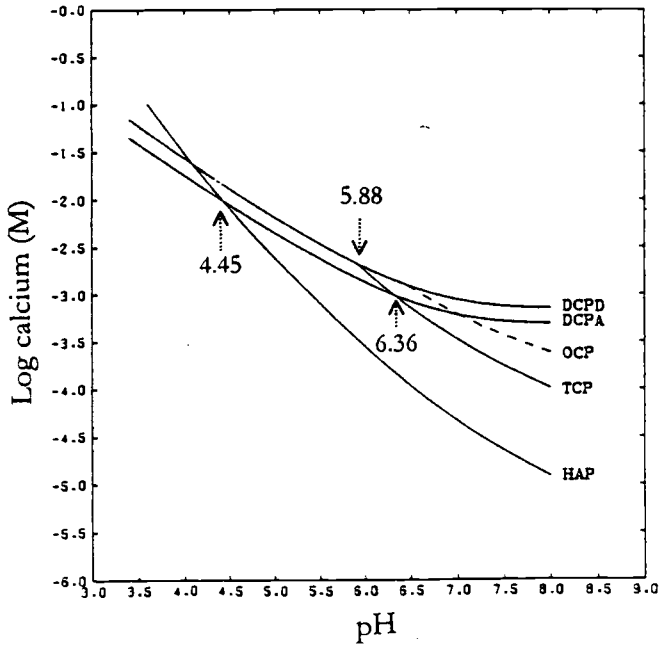

Figure 1. Calculated solubility isotherms at 25 °C illustrating the relative stability of several calcium phosphates. (DCPA in the figure is monetite).

Figure 1 shows that HAP is the most stable phase at pH higher than 4.45. It is also increasingly more stable than other calcium phosphates at higher pH. However, at too high pH (higher than 8.0) calcium hydroxide or $Ca(OH)_2$ tends to form instead. Therefore, pH was kept in the range of 6.5 to 7.5 throughout aging periods to sustain

the HAP domination among all calcium phosphates in both volumetric precipitation and surface nucleation.

MATERIALS

Main materials involved in the experiment were titanium substrates, dihydrogen phosphate dihydrate ($KH_2PO_4 \cdot 2H_2O$), and calcium chloride dihydrate ($CaCl_2 \cdot 2H_2O$). Titanium foil, 2.0 mm thick, 99.7% purity (commercial grade) was supplied by SIGMA. Potassium phosphate (monobasic and anhydrous), 99%, was also supplied by SIGMA, while commercial grade $CaCl_2$ was supplied by Mallinckrodt. An HAP (Lot 97H5236, SIGMA) suspension in 0.001 M phosphate buffer with pH 6.8, was used as a reference for X-ray diffraction (XRD) patterns of HAP.

METHODS

Substrate preparation

Titanium was polished with silicon carbide papers (SiC) grid numbers 240, 320 and 400 from the coarsest to finest. After the surface was polished until smooth and shiny, it was cut into 10 mm × 10 mm samples by jigsaw. All 4 sides of each sample were then polished.

Oxidation

Samples were thoroughly degreased in a soap solution followed by ultrasonication in pure acetone for 30 minutes to remove all organic compounds. They were then soaked in an acid solution (3% HNO_3 + 2% HF + 95% deionized water) for 30 seconds to remove a thin, naturally formed oxide layer, to help strengthen the intentional oxide layer. After each surface preparation step, Ti substrates were rinsed with deionized water for 30 seconds and blown dry with nitrogen gas. Samples were oxidized in a high-temperature furnace as shown in Figure 2 at different temperatures and periods of time. Temperatures used were 600, 610, 700, 800, 900, 1,000, 1,200, 1,300 and 1,500 °C with a 10 °C/minute heating rate. Substrates were oxidized for 10 minutes, 1 hour, or 6 hours. Two systems were studied: a flow system of oxygen and a flow system of simulated air (79% nitrogen gas and 21% oxygen gas). Four substrates were put on a 3 cm × 5 cm alumina tray, which lied horizontally in the middle of the alumina tube of the furnace (38.1 mm diameter, 1,524 mm long with a uniform zone of 130 mm at ± 2 °C). The tube was purged with argon gas during the temperature ramp. When the temperature reached the set point, oxygen and/or nitrogen gas was fed through the reactor tube at a constant flow rate. Oxygen and/or nitrogen gas was shut down immediately after the temperature started decreasing (the end of the oxidation period) and argon gas was turned on for purging in order to completely stop the oxidation. The oxygen flow rate was 1.75 L/min for the oxygen system, and was the same for the simulated air system, with an additional 6.58 L/min of nitrogen gas to achieve the 21/79 O_2/N_2 molecular ratio of natural air.

Reactant gases were turned on only during the period of constant temperature for a controlled constant rate of oxidation.

Solution preparation

Boskey et al. (1976) stated that in the presence of high concentrations of calcium and phosphate (total Ca and total PO_4 each greater than 10 mM) and at pH values greater than 6.5, precipitation of hydroxyapatite is always preceded by the formation of an amorphous precursor. In the presence of lower concentrations of calcium and phosphate (total Ca and PO_4 each less than 2 mM), the first precipitate formed at pH 7.4 had an x-ray diffraction pattern, a morphology, and colloidal properties distinct from those of the amorphous calcium phosphate found in the presence of higher concentrations of reactants. They used $CaCl_2$ and Na_2HPO_4 in their work, with NaOH and HCl to adjust pH.

Supersaturated solutions of phosphate and calcium were prepared from slow mixing of $CaCl_2$ and KH_2PO_4 solutions. A calcium solution was prepared first, then phosphate solution was slowly added into it while keeping pH between 6.5-7.5 with 0.01 M KOH solution, in order to prevent the formation of any calcium-deficient HAP. The total concentration of calcium ions in a final solution was between 1-25 mM while that of phosphate ions was between 0.5-15 mM. These calcium and phosphate concentrations covered all three concentration ranges; low concentration (total Ca and PO_4 each less than 2 mM), intermediate concentration (total Ca and PO_4

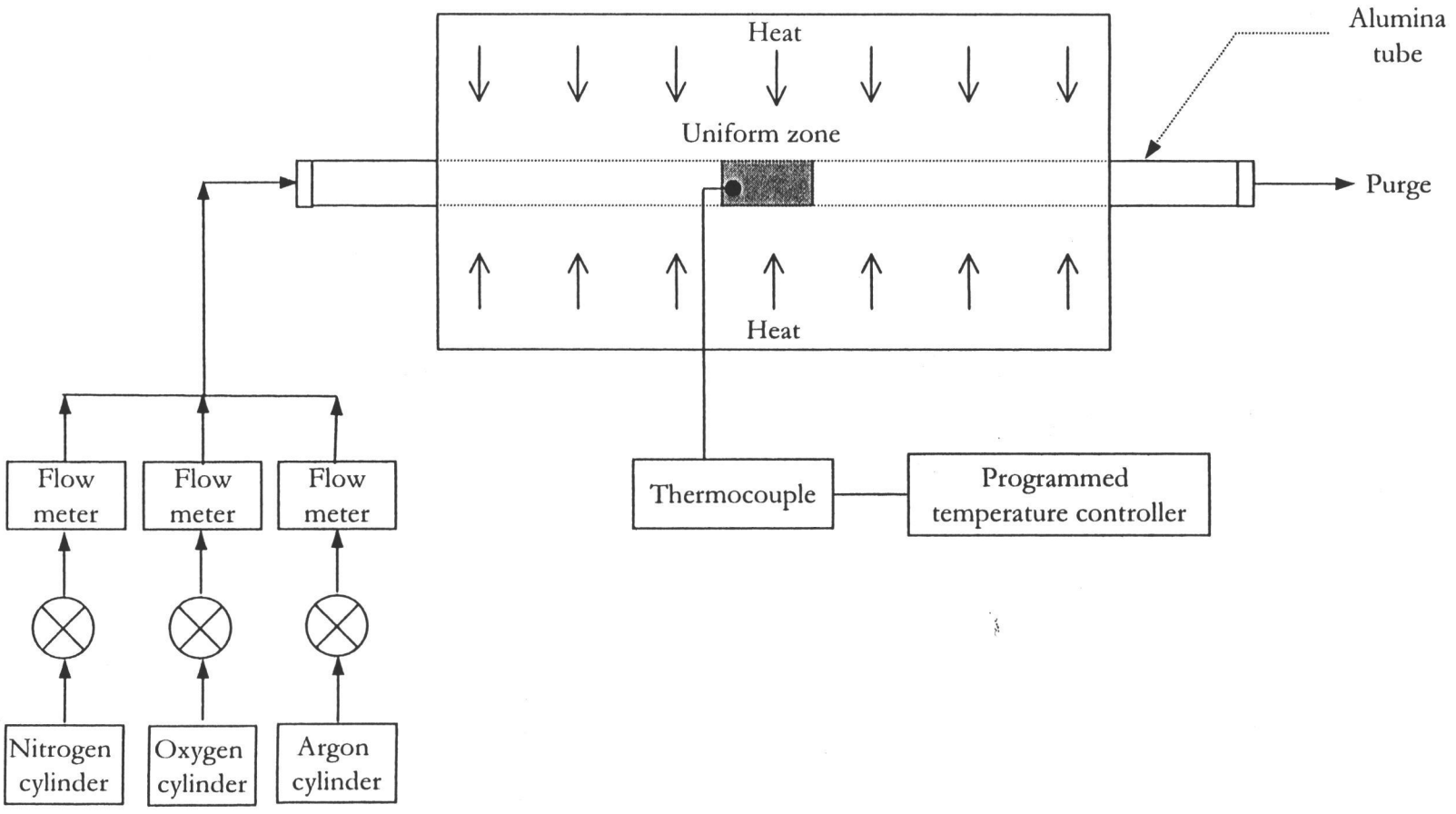

Figure 2. Oxidation system apparatus (not drawn on scale).

each between 2 and 10 mM), and high concentration (total Ca and PO_4 each greater than 10 mM).

Aging

Oxidized substrates were cleaned with acetone in an ultrasonic bath for 30 minutes, rinsed in deionized water for 1 minute, and blown dry with nitrogen gas before being immersed in 200 ml of prepared supersaturated solution for 1 hour to 14 day aging periods. Solutions were kept in a covered glass container at pH between 6.5-7.5 (adjusted with 0.01 KOH solution) and constantly stirred with a Teflon-coated magnetic stirrer at 110-150 rpm.

CHAPTER 3

RESULTS AND DISCUSSION

RESULTS

Analysis

Preliminary experiments involving only supersaturated solutions were done first to find an appropriate concentration for volumetric HAP precipitation. Powder precipitate obtained from volumetric precipitation was tested by X-ray diffraction (XRD, Norelco-12045) with Cu-K_α radiation and 0.05° step size. Later experiments involved aging of oxidized titanium substrates in supersaturated solutions. Prepared surfaces were tested by X-ray photoelectron spectroscopy (XPS, ESCA SSX-100) and Scanning electron microscopy (SEM, Hitachi 4700). A monochromatized Al-K_α X-ray source was used at 20 mA, 10 kV in the XPS apparatus. Corresponding precipitate obtained was tested by a different XRD apparatus (Siemens D5000) with Cu-K_α radiation and 0.02° step size for more precise results.

An XRD pattern for the reference HAP was collected from a commercial HAP powder, shown in Figure 3. The 2θ range (from 24 to 54) contains all main characteristic peaks at 26.0, 31.9, 32.3, 33.0, 34.2, 39.9, 46.7, 49.6 and 53.3. This pattern corresponds to typical XRD patterns of HAP shown by Liu (1997) and Jayne et al. (1999) which ascertains that the correct reference was used.

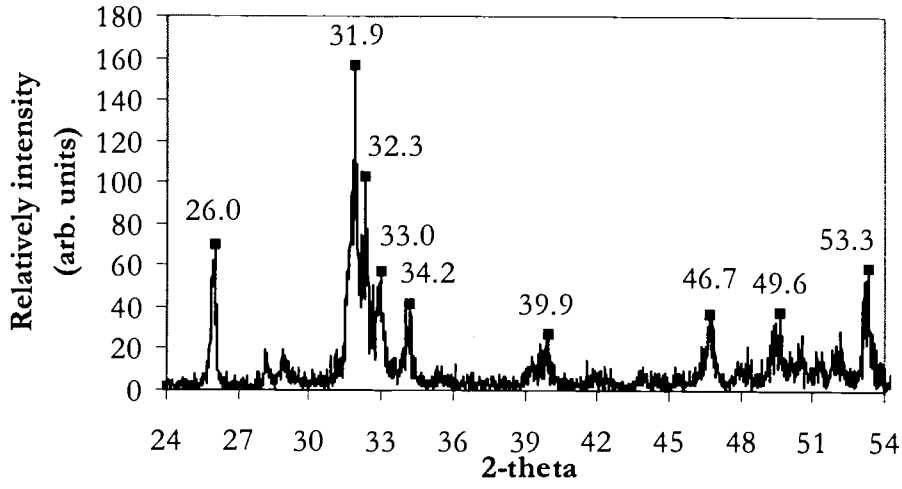

Figure 3. Reference XRD pattern of HAP commercial powder.

Volumetric precipitation

Starting concentrations of phosphate and calcium were always at the stoichiometric ratio of HAP, i.e. Ca/P = 1.67. The first step of the experiment focused on finding the right supersaturated concentration of HAP that could crystallize HAP powder, to be used for surface nucleation in the next step. Table 2 shows three concentrations in three ranges.

Table 2. Calcium and phosphate concentrations of supersaturated solutions.

Ca^{2+} conc. (mM)	PO_4^{3-} conc. (mM)	Ca/P	Concentration	Conc. range
2.00	1.20	1.67	both < 2 mM	Low
9.10	5.45	1.67	2 mM < both < 10 mM	Intermediate
20.73	12.43	1.67	both > 10 mM	High

These concentrations represent three ranges: low, in which both concentrations are less than 2 mM, intermediate, in which both concentrations are between 2 and 10 mM, and high, in which both concentrations are greater than 10 mM. They will be referred to as low, intermediate and high concentration ranges, respectively. The first visible precipitate was formed after 2 hours of mixing calcium and phosphate solutions at the low concentration, and immediately at the intermediate and high concentrations.

Figure 4(c) shows an XRD pattern of precipitate obtained at low concentration, and is very well matched with the reference HAP at all main peaks. The XRD patterns of precipitate obtained at high and intermediate concentrations (Figure 2(a) and 2(b)) show the biggest peak at 28.0-28.2, corresponding to a main characteristic peak of TCP (Liu, 1997; Jayne et. al., 1999). They also have some characteristic peaks of HAP at 2θ between 31.0-34.0, but not with the exact same intensity and pattern as those of HAP. These patterns show that a mixture of TCP and HAP crystallized at the intermediate and high concentrations but only HAP precipitate crystallized at the low concentration.

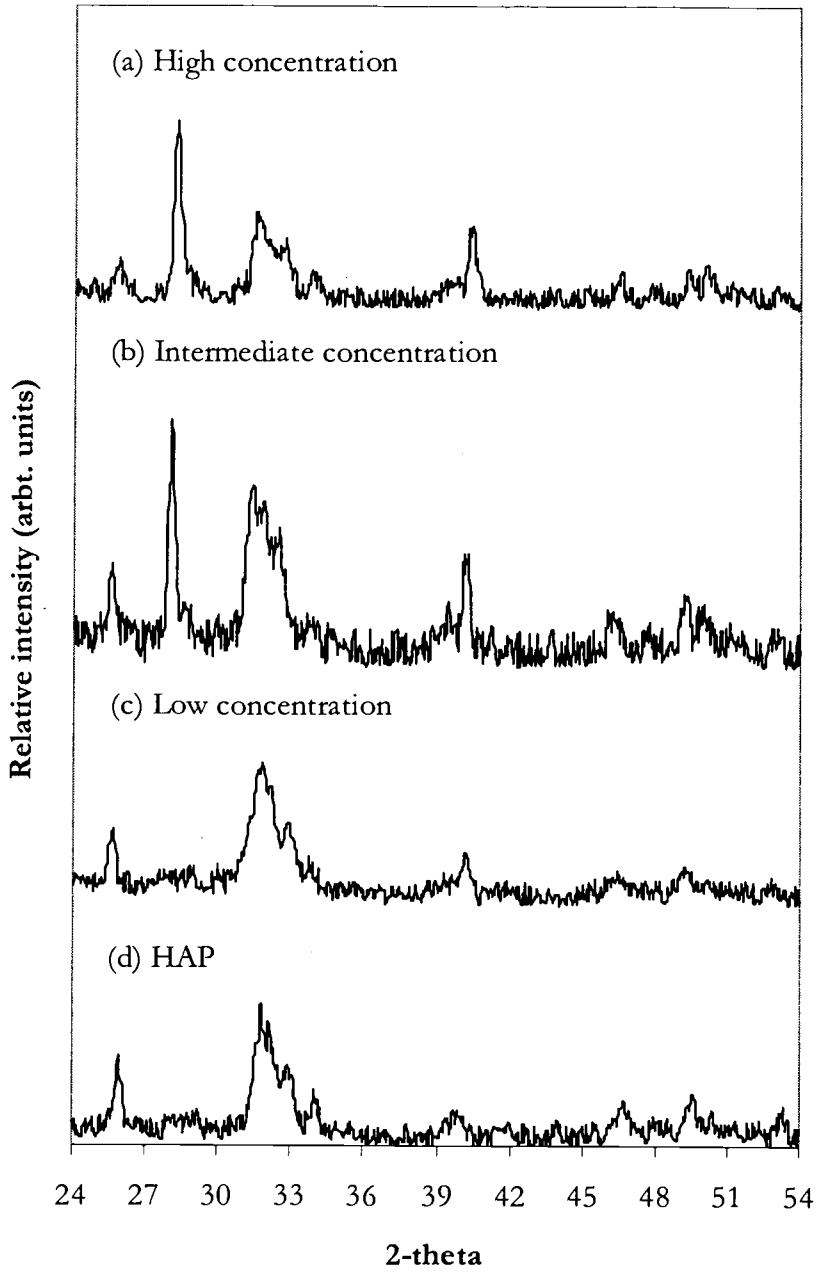

Figure 4. XRD patterns of (a) precipitate at high concentration; (b)precipitate at intermediate concentration; (c) precipitate at low concentration and (d) reference HAP.

As of yet, there is no certain explanation of the formation of the TCP and HAP mixture at intermediate and high concentrations. However, TCP, with a Ca/P ratio of 1.50, is also known as a transformation of calcium-deficient HAP (Fanovich et al., 1998). In their work, they synthesized HAP from 0.52 M H_3PO_4 and 0.87 M $Ca(OH)_2$, which are at high concentrations. Zhang et al. (1997) also found a mixture of TCP and HAP synthesized from 0.32 M $(NH_4)_2HPO_4$ and 0.54 M $Ca(NO_3)_2$, which are at high concentrations. In their work, it has been found that an addition of 0.02 M polyacrylic acid (MW 2,000) in the starting precipitate helps stabilize HAP. There is a possibility that when concentrations of calcium and phosphate are higher than 2 mM, the volumetric reaction occurs too rapidly. HAP formation requires transformation from other forms of calcium phosphates with lower Ca/P ratios. Solutions at low concentrations provide better conditions for slower reactions, which enhance the likelihood of transformation from other phases of calcium phosphates to HAP.

Attention was paid to the low concentration solution after its XRD pattern showed the best match with HAP among all concentration ranges. After all phosphate-containing solution was added to the calcium-containing solution, the pH was fairly constant until the first visible precipitate formed after about 2 hours, then pH decreased gradually due to the crystallization of precipitate in the solution. After about 5 hours, pH started leveling off naturally at around 6.6-6.8. From then on, a few drops of 0.01 M KOH were added every 12 hours to maintain pH no less than 6.5, which will sustain the HAP domination among all calcium phosphates. It showed that HAP first formed after about 2 hours and the precipitation slowed down after 5 hours.

Surface nucleation

After obtaining the concentration for the volumetric precipitation of HAP, the next step was the Ti substrate preparation for HAP surface nucleation. Titanium substrates were oxidized in O_2 at different temperatures, from 600-1,500 °C. Table 3 shows the morphology of oxide layers after oxidation for 6 hours at different temperatures. At temperatures higher than 800 °C, the oxide becomes very thick (rapid oxidation) with a high tendency to flake off.

Table 3. Visual morphology of oxide layers oxidized in O_2 at different temperatures for 6 hours.

Temp.(°C)	Morphology	Adhesion
600, 610	very smooth, slate-gray	extremely adherent to metal
700	Smooth, blue-gray	adherent to metal
800	smooth, light gray with some white spots	start having tendency to flake of
900	uniform yellow-white	fairly easy to flake off
1100	Orange-brown	very easy to flake off
1300	rough, shiny golden-orange	very easy to flake off, brittle
1500	very rough (big grain), shiny maroon	very easy to flake off, very brittle

Soten et al. (1999) have implied that the co-existence of both the rutile and anatase phases of TiO_2 plays an important role in the surface nucleation of HAP. The phase diagram for the Ti-TiO_2 system, shown later in Figure 10, suggests that a temperature below 800 °C is appropriate for forming both phases.

Oxide layers from low temperature oxidation (610 °C) were studied due to their strong adhesion with Ti substrates and their tendency to form both the anatase

and rutile phases of TiO_2 on the surface. The oxidation rate at temperatures below 500 °C is too slow which was another reason why temperature at 610 °C was chosen. Phases of TiO_2 will be discussed later in this chapter. After oxidation, all substrates were immersed in three different solutions (corresponding to those shown in Table 2).

Figure 5(a) shows a scanning XPS spectrum from binding energy 0 to 1,000 eV of Ti substrate after polish and cleaning steps. Corrected (from C 1s peak calibration) main peaks are only O 1s at 529.9, Ti 2p at 457.6 and C 1s at 284.6. Figure 5(b) shows the spectrum of the substrate surface after oxidation in oxygen at 610 °C for 1 hour. It has three of the same main peaks but with a significantly larger O 1s peak than that of the surface before oxidation. Small C 1s and O 1s peaks are always present from carbon and oxygen atoms in the atmosphere. Based on the equation proposed by Unnam et al. (1986) for the Ti-oxidation with O_2, the estimated thickness for oxidation at this temperature for 1 hour is 134.5 nm.

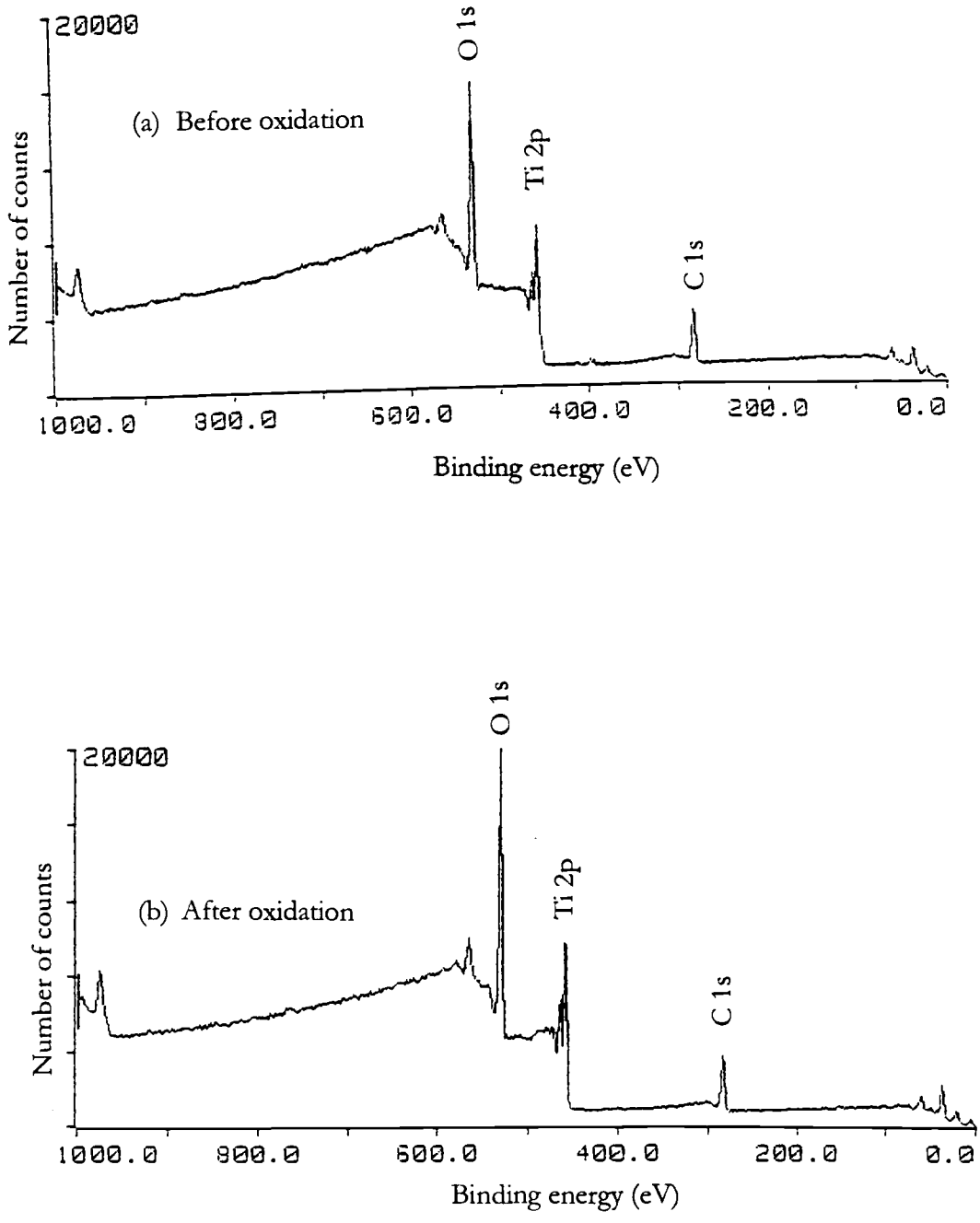

Figure 5. Scanning XPS spectra of titanium substrates (a) before oxidation and (b) after oxidation in oxygen at 610 °C for 1 hour.

Substrates treated at different temperatures were immersed in different solutions with different aging periods. Samples oxidized in O_2 at 610 °C for 1 hour and at 800 °C for 10 minutes were immersed in a solution used by Soten et al. (1999). The solution was at very low concentration of 0.16 mM Ca^{2+} and 7.6 mM PO_4^{3-} with Ca/P ratio 0.02, far less than that of HAP. In such a calcium-deficient solution, the XPS analysis of both substrates showed only 4% concentration of P on surface with zero Ca after aging for 10 days. This shows the invalidity of the solution for HAP nucleation on thermally treated Ti substrates.

Some substrates oxidized in O_2 at 610 °C for 1 hour were immersed in non-stochiometric solutions of 7.6 mM PO_4^{3-} with 3.7 mM and 7.6 mM Ca^{2+} for Ca/P ratio 0.5 and 1.0, respectively. Both of those solutions were in the intermediate concentration range as defined in Table 2. Surprisingly, for those calcium-deficient solutions, only Ca was found on the surface with 3% atomic concentration while no P was found, after aging for 10 days.

Atomic percents and binding energy from XPS analysis of selected substrates in different solutions are displayed in Table 4. All solutions used were at the stoichiometric Ca/P ratio in different concentration ranges corresponding to those shown in Table 2. Positive energy shift calibrated with C 1s peak shows that there is an insulating layer on top of the metal substrate. Higher energy shift is from a thicker insulating layer on the surface that can come from oxide or HAP. Samples A, B, and C are only plain surfaces without being aged in any solution. Sample A was the starting plain Ti substrate (after polish and cleaning steps) corresponding to the survey scan spectrum in Figure 5(a).

Table 4. XPS analysis of different substrates in different solutions.

Sample	Surface Treatment	Solution	Aging time (days)	Atomic concentration (%)				Ca/P ratio	C1s binding energy shift (eV)	Corrected binding energy (eV)			
				P	Ca	Ti	O			P	Ca	O	Ti
A	Plain Ti	No	--	0	0	13.1	45.7	--	+ 0.7	--	--	529.9	457.6
B	610 °C, 1 hr, O_2	No	--	0	0	11.4	55.3	--	+ 0.9	--	--	529.4	458.4
C	610 °C, 1 hr, Air	No	--	0	0	11.7	53.6	--	+ 0.8	--	--	529.7	458.5
D	610 °C, 1 hr, O_2	Low conc.	10	12.7	21.1	0	54.5	1.66	+ 5.9	132.9	346.8	530.6	--
E	610 °C, 1 hr, O_2	Interm. Conc.	10	0	3.7	16.1	59.9	--	+ 0.8	--	347.6	529.6	458.3
F	610 °C, 1 hr, O_2	High conc.	10	2.9	3.1	23.1	55.8	1.07	+ 2.9	131.6	345.7	527.6	456.6
G	610 °C, 1 hr, O_2	Low conc.	0.5 (12 hrs)	13.0	18.2	0	54.7	1.41	+ 3.7	132.8	346.7	530.6	--
H	610 °C, 1 hr, O_2	Low conc.	2	10.9	17.8	0	57.7	1.62	+ 4.1	132.7	346.6	530.5	--
I	610 °C, 1 hr, O_2	Low conc.	5	12.2	19.9	0	56.1	1.63	+ 5.3	132.8	346.7	530.5	--
J	Plain Ti	Low conc.	10	2.3	2.1	17.7	40.5	0.92	+ 1.0	132.9	347.0	532.4	458.2
K	610 C, 1 hr, Air	Low conc.	10	14.4	18.5	0	51.1	1.29	+ 4.7	133.0	346.8	530.7	--

Samples D, E, and F were oxidized in O_2 at 610 °C for 1 hour but were aged in different solutions at the stoichiometric ratio of HAP. At the high concentration, there was some Ca and P coated on the surface with a Ca/P ratio of only 1.07, which is far less than the Ca/P ratio of HAP (1.67). The Ti concentration was still high, which showed an incomplete coating on the surface. At the intermediate concentration, only calcium was found without any phosphate, with much Ti still remaining on surface. At the low concentration, titanium concentration went to zero while Ca and P compositions were high with a Ca/P ratio of 1.66, which is very close to the Ca/P ratio of HAP.

Figures 6(a) and 6(b) respectively display 6,000X magnification and 15,000X magnification SEM images of sample D, oxidized in O_2 at 610 °C for 1 hour and aged in the low concentration solution for 10 days. The images show morphology of the coated surface with HAP coverage as rose-like structures. Those rose-like structures are like the HAP structures shown in Soten et al. (1999) and unlike the pure TiO_2 structures of round white clumps shown in Narayana et al. (1998), which ascertains the formation of HAP on oxidized surface. There are two possibilities for the identity of the big white islands shown in both pictures. First, they might be the beginning of the next layer growth of HAP, on top of the rose-like structures. Secondly, the mechanism for HAP surface nucleation might have changed over the period of 10 days, so the islands could be the beginning of the formation of some other forms of calcium phosphates.

(a)

(b)

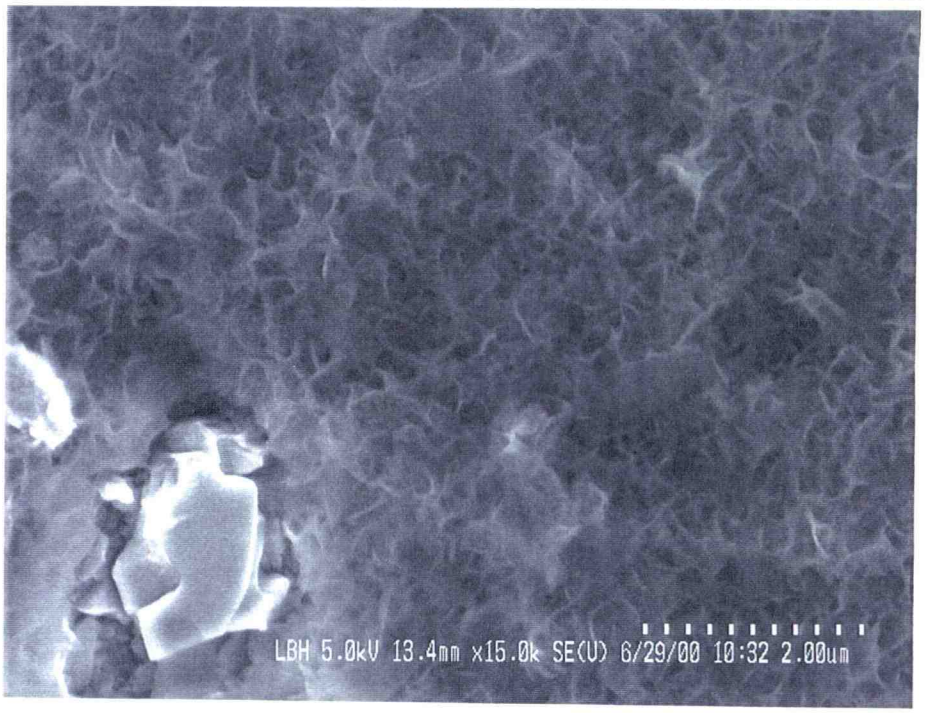

Figure 6. SEM images showing morphology of grown HAP on a titanium substrate, after immersion in the low concentration solution for 10 days (a) 6,000X magnification and (b) 15,000X magnification.

Figure 7 shows XRD patterns of precipitate simultaneously formed in solutions used to nucleate HAP on surface. Figure 7(a) shows the XRD pattern of precipitate at the high concentration (sample F); Figure 7(b) shows that of precipitate at the low concentration (sample D) and Figure 7(c) shows that of reference HAP. The spectrum in Figure 7(b) is very well matched to that of HAP. It is concluded that HAP is formed, covering the entire surface of the substrate after oxidation in oxygen at 610 °C for 1 hour, during a 10-day aging process in a low concentration solution. This conclusion is from observing a good atomic ratio of Ca/P and finding zero percent of It remaining on the surface from XPS analysis, observing SEM image of surface morphology, and analyzing the XRD pattern of the corresponding precipitate.

Percent yield was calculated from the percent of number of moles of HAP obtained in precipitate per 10 moles of Ca put in (from the stoichiometric ratio of 10 moles of Ca per 1 mole of HAP. The average percent yield of volumetric precipitation without immersed substrates was 45.2 and 60.5 at low and high concentration, respectively. The average percent yield of volumetric precipitation with immersed substrates was 28.7 and 59.4 at low and high concentration respectively. The significant decrease in percent yield when substrates were immersed in the low concentration solution also confirmed the surface nucleation of HAP.

Figure 8 compares the Ca/P ratios of the coated surface for samples G, H, I, and D, oxidized in O_2 at 610 °C for 1 hour and aged in the same low concentration solution for 12 hours, 2 days, 5 days and 10 days respectively. After aging for 12 hours, the whole oxide surface was completely covered with some Ca and P, which can be seen from zero Ti atomic concentration and the rising Ca and P concentrations from zero

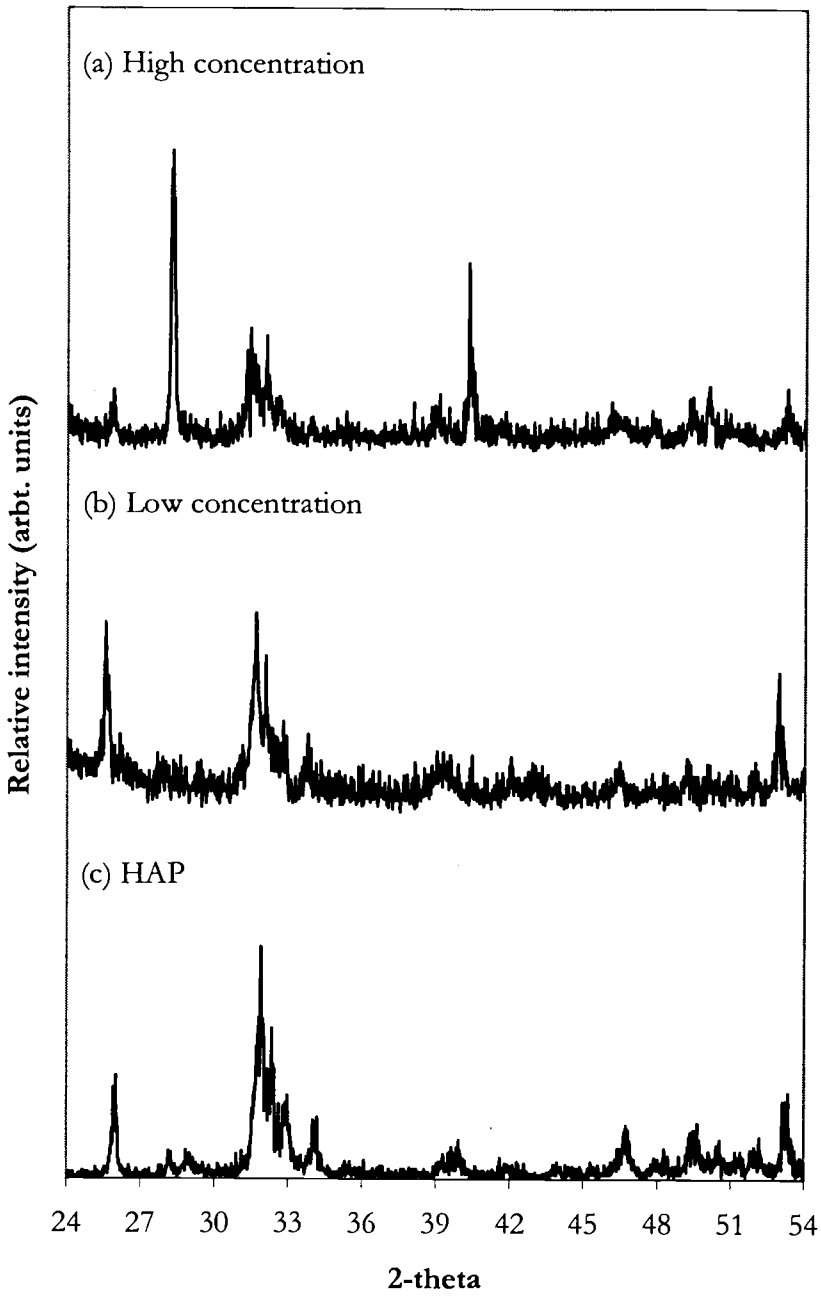

Figure 7. XRD patterns of (a) precipitate at high concentration; (b) precipitate at low concentration and (c) reference HAP.

shows the spectrum of sample D, where the Ti 2p peak disappears and large Ca 2p and P 2p peaks are clearly seen.

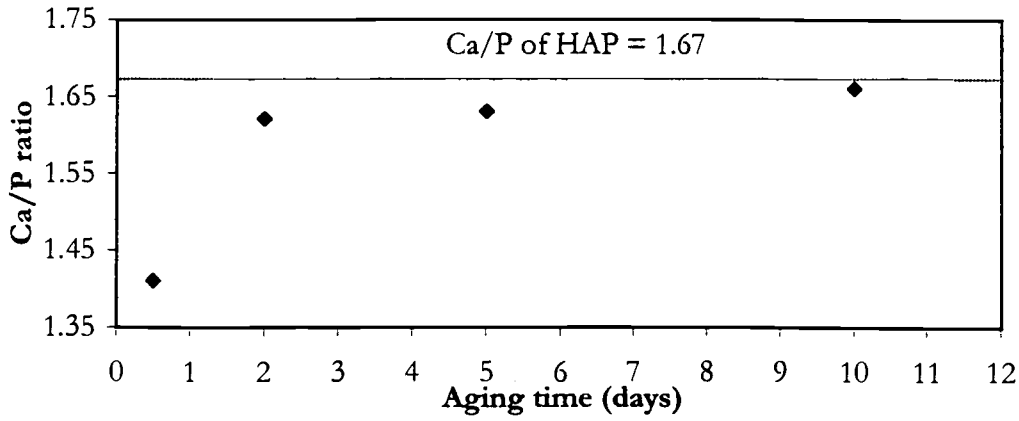

Figure 8. Change in Ca/P ratio with time for substrates oxidized in O_2 at 610 °C for 1 hour, low concentration solution.

For better comparison, XPS analysis from aging in the low concentration solution of plain It, and It oxidized in simulated air at 610 °C for 1 hour is also shown as samples J and K, respectively. Results of plain Ti obviously showed an incomplete coverage with very low P and Ca concentrations at a low Ca/P ratio. Figure 9(a) shows that the scanning XPS spectrum of sample J, obtained from plain Ti, is not much different from the spectrum in Figure 5(a) of non-oxidized (untreated) Ti, with very small Ca 2p and P 2p peaks at 347.0 and 132.9 eV, respectively. Figure 9(b) shows the spectrum of sample D, where the Ti 2p peak disappears and large Ca 2p and P 2p peaks are clearly seen.

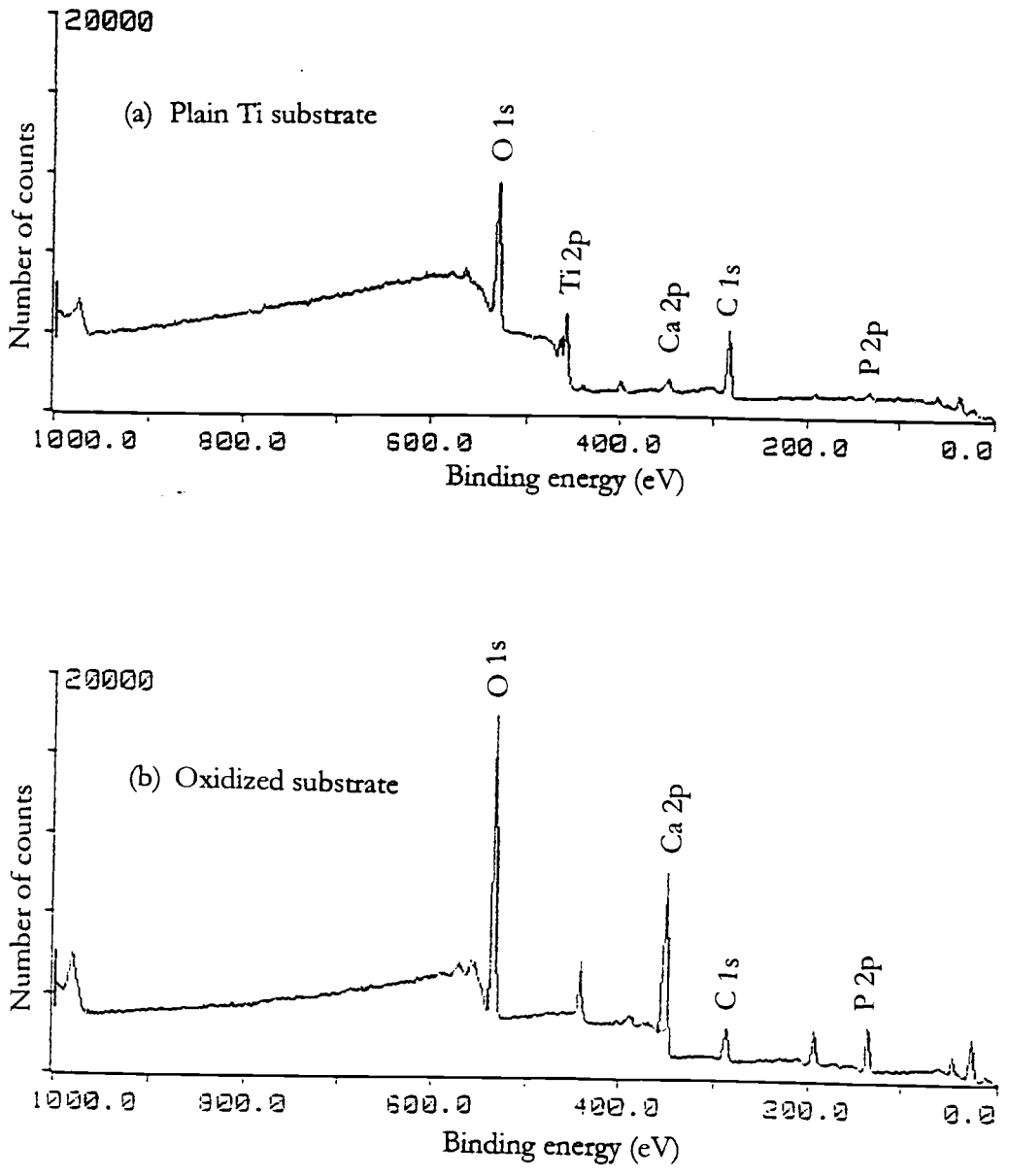

Figure 9. Scanning XPS spectra of substrates after aging in low concentration solution for 10 days (a) plain Ti substrate and (b) oxidized in O_2 at 610 °C for 1 hour.

For sample K, oxidized in air, the surface was also completely covered after 10 days but with a Ca/P ratio of 1.29, much lower than that of HAP. Some other substrates, oxidized in simulated air at 800 °C and 900 °C for 10 minutes, were also immersed in a solution at the same low concentration, aged for 10 days. No P or Ca was found on the surface at either oxidation condition from the XPS analysis. All this confirms the necessity of the oxide layer formed in O_2 at low temperature, to enhance HAP nucleation on the Ti surface.

The study of volumetric precipitation and surface nucleation of HAP has indicated that they correspond to each other. At the low concentration, HAP crystallized in solution and the surface composition showed total coverage, with a Ca/P ratio close to that of HAP. At the intermediate concentration, a mixture of HAP with TCP crystallized in the solution and no phosphate coated the surface; only Ca was attracted to the surface. At the high concentration, impure HAP also crystallized in the solution and some Ca and P were found on the surface, but with a Ca/P ratio far lower than that of HAP.

DISCUSSION

The crystal structure of HAP belongs to the space groups $P6_3/m$ in the hexagonal system with the lattice parameters, a (= b) = 0.9432 nm and c = 0.6881 nm. Details of the HAP structure and a picture of the HAP unit cell are shown in the appendix.

Ti-TiO_2 system

The phase diagram of the Ti-TiO_2 system (Hauff, 1965) is shown in Figure 10. According to Hauff, at intermediate temperatures (up to 800 °C) the scaling layer appeared to consist almost entirely of TiO_2. Above 800 °C, especially after long oxidation times, TiO formed in the immediate neighborhood of the metal phase, and in the middle region of the scaling layer, Ti_2O_3 was observed in addition to TiO_2.

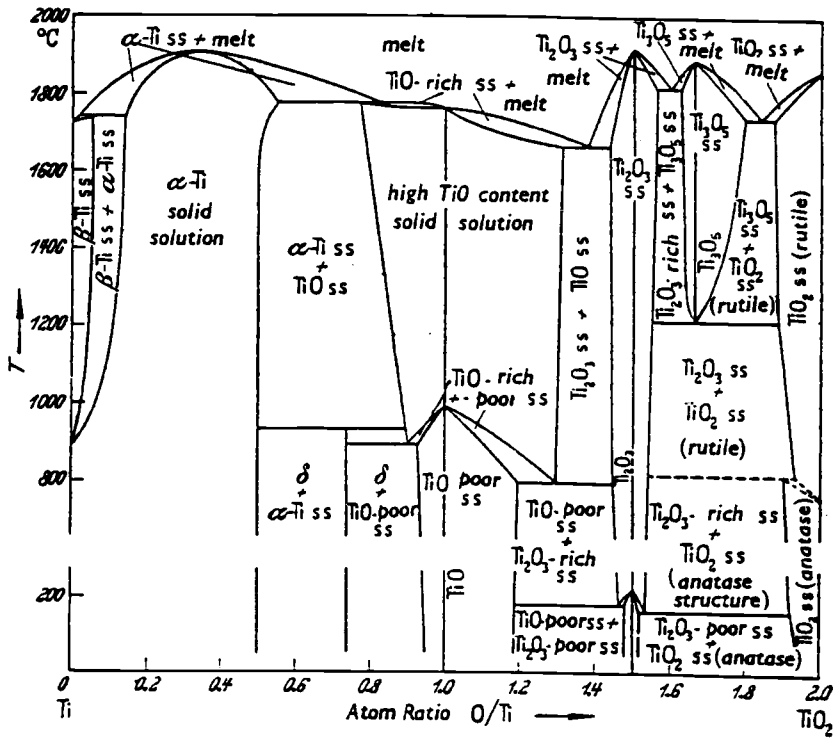

Figure 10. Phase diagram for the Ti-TiO_2 system (ss denotes solid solution).

The three phases of TiO_2 are rutile, anatase, and brookite, as shown in Table 5. Rutile is the most thermodynamically stable. Nevertheless, the lattice energies of the

other phases are similar and hence are stable over long periods. Above 700 °C, the monotropic conversion of anatase to rutile takes place rapidly. Brookite is difficult to produce and therefore is not of much interest in TiO_2 production. In all three TiO_2 modifications, one titanium atom in the lattice is surrounded octahedrally by six oxygen atoms, and each oxygen atom is surrounded by three titanium atoms in a trigonal arrangement. The three phases correspond to different ways of linking the octahedra at their corners and edges. Crystal lattice constants and densities of the three phases of TiO_2 are given in Table 5 (Anderson et al., 1957; Buxbaum, 1993).

Table 5. Crystallographic data for TiO_2 phases.

Phase	Crystal System	Lattice Constant (nm)			Density (g/cm^3)	Hardness (Mohs)
		a	B	C		
Rutile	Hexagonal	0.4597	--	0.2958	4.21	6.5-7.0
Anatase	Tetragonal	0.3785	--	0.9514	4.06	5.5
Brookite	Rhombic	0.9184	0.5447	0.5145	4.03	N/A

Devries et al. (1954) stated that regarding the conversion of anatase to rutile, it is a moot point whether anatase has any stable region of existence or whether it is completely metastable with respect to rutile at all temperature. Although a temperature of 700-800 °C is required to convert anatase to rutile, the thermodynamic data and experimental evidence, such as the reported precipitation of rutile at room temperature under certain conditions, indicates that rutile is the stable phase throughout the temperature range from room temperature to its melting point. The high conversion rate, demonstrated by the relatively easy reduction of anatase, is

shown as dashed lines in Figure 10. The cooling after constant temperature oxidation was done slowly at 10 °C/min, until the temperature returned to room conditions by purging with argon gas. From the phase diagram, anatase is stable at temperatures lower than 800 °C in a system with oxygen only. When the temperature cools down slowly in an inert gas system, there is a tendency for some anatase to convert to rutile when the temperature approaches room conditions. All this information leads to the conclusion that oxide layers formed in a O_2 system at relatively low temperatures (below 700 °C) have a good potential to consist of both the anatase and rutile phases.

Anatase

Anatase TiO_2 has a crystal lattice matching that of HAP. The arrangement of OH groups on the (110) oriented TiO_2 layer along $[001]_{anatase}$ shows excellent one-dimensional (1-D) coherent matching with the (0001) plane of HAP along $[0110]_{HA}$ as illustrated in Figure 11 (Mao et al., 1998). The dashed and bold line frames show the outlines of the unit cells of HAP along (0001) plane and TiO_2 along (110) plane respectively.

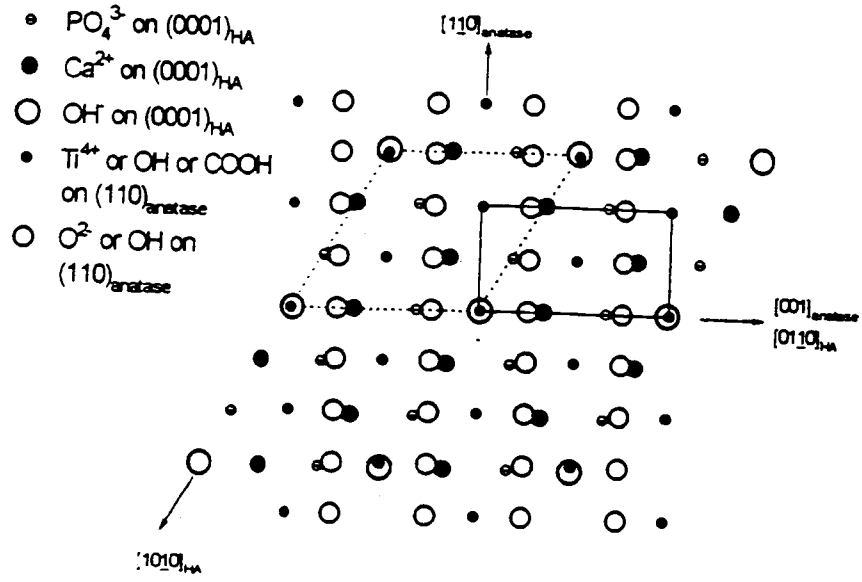

Figure 11. Lattice matching between OH group of TiO_2 layer and HAP plane.

Rutile

Rutile TiO_2 is known to be hydroxylated, and Bronsted acid and base hydroxyl sites exist at the surface. Figure 12(a) shows the O 1s peak of a substrate after oxidation in oxygen at 610 °C for 1 hour. The binding energy as shown needs to be corrected by adding 0.9 from the C 1s peak calibration. There are three main peaks, the largest at 530.3 eV, the medium at 532.6 eV, and the smallest at 531.8 eV.

Sham et al. (1979) stated that for various hydrated and clean rutile TiO_2 single crystals, two types of surface OH species are present, Ti-OH and OH(s), as well as molecular H_2O overlayers on the ambient hydrated surface. The O 1s spectrum of TiO_2 has three peaks; the one at the highest binding energy corresponds to Ti-OH, or basic sites, the one at next lower binding energy corresponds to OH(s), or acidic sites,

and the one at the lowest binding energy is the bulk H_2O overlayer. Acidic sites, or OH(s), and basic sites, or metal-OH, are both formed from H_2O chemisorption and exist on TiO_2.

Acidic sites are able to attract negatively charged species while basic sites are able to attract positively charged species, which are PO_4^{3-} and Ca^{2+}, respectively, in this case. A schematic illustration of the rutile TiO_2 unit cell with acidic and basic hydroxyl groups as shown in the appendix.

Figure 12(b) shows the O 1s peak of the substrate that had been immersed in the low concentration for 10 days (corresponds to sample D in Table 4). The binding energy as shown needs to be corrected by adding 5.9 from the C 1s peak calibration. It shows the only oxygen peak remaining was at the lowest binding energy (530.6 eV), which corresponds to the bulk H_2O layer, while Ca acidic and basic sites of the two higher O 1s peaks have disappeared.

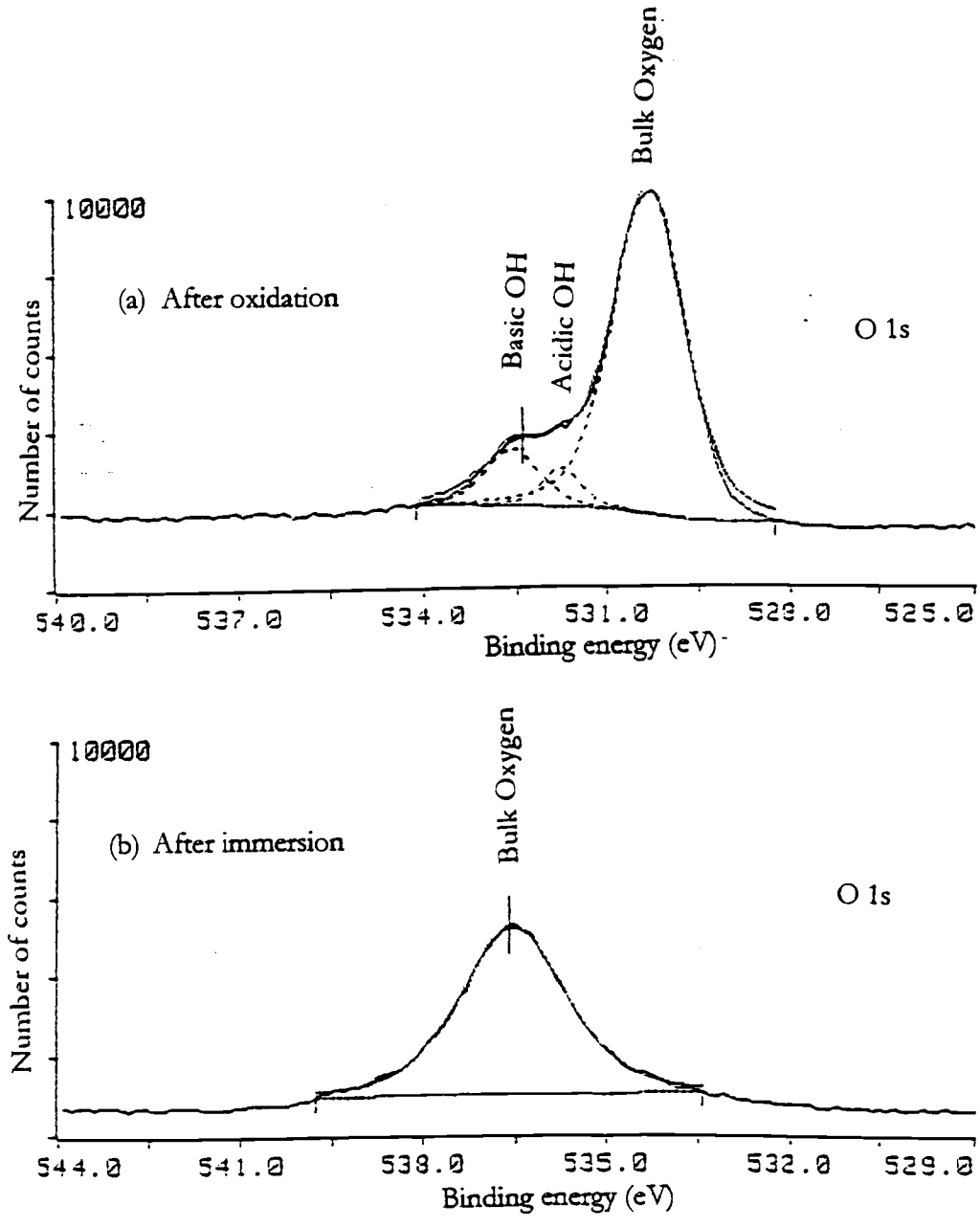

Figure 12. Spectra of O 1s peaks (a) after oxidation at 610 °C for 1 hour in oxygen (add 0.9 for correction) and (b) after immersion in the low concentration solution for 10 days (add 5.9 for correction).

From the lattice matching between OH groups of the anatase TiO_2 layer and HAP plane, and the XPS analysis of O 1s peaks on rutile TiO_2, it is convincing that a mixture of rutile and anatase TiO_2 (from an oxidation in O_2) on Ti substrates helps the HAP surface nucleation.

There is still no certain explanation of why the oxide layer from oxidation in simulated air does not enhance HAP surface nucleation. However, from the phase diagram shown in Figure 10 was derived from experimental data of oxidation in O_2 and a naturally formed oxide layer at room temperature appears to be entirely rutile (Bullock et al., 1996). There is a possibility that only rutile TiO_2 is formed from the oxidation in simulated air at relatively low temperature. Rutile is able to attract some Ca^{2+} and PO_4^{3-} but by itself is not sufficient to enhance HAP surface nucleation. From the phase diagram, the atomic ratio of O/Ti must be greater than 1.5 to enter the region of anatase TiO_2. It is possible that a simulated air system results in an oxygen-deficient oxidation, which enhances the formation of an oxide layer outside the region of the anatase phase.

CHAPTER 4

CONCLUSION

The surfaces of titanium substrates were successfully coated with HAP when the titanium substrates were oxidized in oxygen at 610 °C for 1 hour, and aged in a supersaturated solution of 1.20 mM PO_4^{3-} and 2.00 mM Ca^{2+} (starting Ca/P ratio = 1.67). After aging for 2 days, XPS analysis showed Ti, Ca, and P surface concentrations of 0.0%, 17.8%, and 10.7% respectively, with a Ca/P ratio of 1.62. The total coverage of HAP on the oxide layer was demonstrated by a Ti surface concentration of zero. After aging for 10 days, the surface concentration of Ca went up to 21.1% and that of P went up to 12.7% with a Ca/P ratio of 1.66. The corresponding SEM images, at 6,000X and 15,000X magnification, show HAP coverage on the surface as rose-like structures.

XRD patterns of simultaneously crystallized powder from the solution were very well matched with that of the reference HAP. At concentrations of both calcium and phosphate higher than 2 mM, a mixture of HAP and TCP crystallized in volumetric precipitation. There was no HAP detected on the surface of titanium oxidized in air at temperatures ranging from 600 to 900 °C. The presence of both anatase and rutile TiO_2 after thermal oxidation in O_2 at low temperature is believed to enhance the HAP surface nucleation.

CHAPTER 5

FUTURE WORK

This paper showed good results of HAP surface nucleation after Ti substrates were thermally oxidized in O_2 at relatively low temperature (610 °C). Further work can be done in testing shear strength of the coated HAP, observing surface morphology at longer aging periods, and finding the thickness profile with increasing aging time.

There are a few promising methods people have used to produce bulk porous HAP (not coated on metal surface) that can inspire some ideas for coating a thick porous layer on the thin uniform layer successfully formed in this work. This thick layer will be easier to form on a Ti surface totally covered with HAP than on a bare Ti surface, due to its molecular recognition.

Rejda et al. (1977) synthesized porous bioceramic by mixing HAP slurry with hydrogen peroxide (H_2O_2). HAP products had pore sizes over the ranges of 0.5-1.5 μm (microporosity, defined as pore size smaller than 5 μm) and 150-250 μm (macroporosity, defined as pore size greater than 100 μm) that were controlled by varying the hydrogen peroxide concentration.

Liu et al. (1997) used poly vinyl butyral (PVB), particle size of 0.093 mm, 0.188 mm, and 0.42 mm, as a porosifier. Up to 32% of pores greater than 5 μm and 39% of

pores smaller than 5 μm with total porosity of 71% by volume were found in the synthesized HAP blocks.

BIBLIOGRAPHY

1. Abe Y.; Kokubo, T.; Yamamuro, T. Apatite Coating on ceramics, metals and polymers utilizing a biological process *J. Meter. Sci. Mater. Med.* (1)233-238 (1990).

2. Andersson, S.; Collen, B.; Kruuse, G.; Kuylenstierna, U.; Magneli, A.; Pestmalis H.; Asbrink, S. Identification of titanium oxides by X-ray powder patterns. *Acta Chem. Scand.* (11):1641-1657 (1957).

3. Boskey, A.L.; Posner, A.S. Formation of Hydroxyapatite at Low Supersaturation. *J. Phys. Chem.* (80):40-46 (1976).

4. Bullock, E.L.; Patthey, L.; Steinemann, S.G. Clean and hydroxylated rutile TiO_2(110) surfaces studied by X-ray photoelectron spectroscopy. *Surf. Sci.* (352-354):504-510 (1996).

5. Buxbaum, G. I*ndustrial Inorganic Pigments.* Weinheim, New York pp.43-45 (1993).

6. Campbell, A.A.; Graff, G.L.; Song, L.; Sump, K.R. Bioactive void metal composites for orthopedic implant devices. *Mat. Res. Soc. Symp. Proc.* (414):177-182 (1996).

7. Daw, R.; Brook, I.M.; Devlin A.J.; Short R.D.; Cooper, E.; Leggett, G.J. A comparative study of cell attachment to self assembled monolayers and plasma polymers. *J. Mater. Chem.* (8):2583-2584 (1998).

8. Devries, R.C.; Roy, R. A phase diagram of the system Ti-TiO_2 constructed from data in the literature. *Am. Cer. Soc. Bull.* 33(12):370-372 (1954).

9. Ellies, L.G.; Nelson, D.G.A.; Featherstone, J.D.B. Crystallographic changes in calcium phosphates during plasma-spraying. *Biomaterials* 13(5):313-316 (1992).

10. Fanovich, M.A.; Lopez, J.M.P.; Influence of temperature and additives on the microstructure and sintering behavior of hydroxyapatite with different Ca/P ratios. *J. Mater. Sci. Mater. Med.* (9):53-60 (1998).

11. Filiaggi, M.J.; Pilliar, R.M.; Yakubovich, R.; Shapiro, G. Evaluating sol-gel ceramic thin films for metal implant application I Processing and structure of zirconia films on Ti-6Al-4V. *J. Biomed. Mater. Res.* (33):225-238 (1996).

12. Gregory, T.M.; Moreno, E.C.; Patel, J.M; Brown, W.E. Solubility of β-$Ca_3(PO_4)_2$ in the system $Ca(OH)_2$-H_3PO_4-H_2O at 5,15,25 and 37 °C. *J.Res.Nat.Bur.Stand.(U.S.)* 78A(6):667-675 (1974).

13. Han, Y.; Xu, Kewei Morphology and composition of hydroxyapatite coatings prepared by hydrothermal treatment on electrodeposited brushite coatings. *J. Meter. Sci. Mater. Med.* (10)243-248 (1999).

14. Hata, K.; Kokubo, T. Growth of a bonelike apatite layer on a substrate by a biomimetic process *J.Am. Ceram. Soc.* 78(4):1049-1053 (1995).

15. Hauff, K *Oxidation of Metal.* Premium Press, New York. (1965).

16. Jayne, W.F; Moor Jr.,P.A.; Miller, D.M. Solubility and ion activity products of calcium phosphate minerals. *J. Environ. Qual.* (28)530-536 (1999).

17. Kanazawa, T. *Inorganic Phosphate Materials.* Elsevier, Amsterdam, pp.24-25 (1989).

18. King, D.E.; Czanderna, A.W. $^3He^+$ ISS of 11-mercaptoundecanoic acid self-assembled monolayers onto gold. *Surf. Sci. Lett.* (235):L239-L332 (1990).

19. Kokubo, T.; Miyaji, F.; Kim, H. Spontaneous formation of bone-like apatite layer on chemically treated titanium metals. *J. Am. Ceram. Soc.*, 79(4):1127-1129 (1996).

20. Kurzweg, H.; Heimann, R.B. Adhesion of thermally sprayed hydroxyapatite-bond-coat systems measured by a novel peel test. *J. Meter. Sci. Mater. Med.* (9):9-16 (1998).

21. Liu, D.-M. Fabrication of hydroxyapatite ceramic with controlled porosity. *J. Meter. Sci. Mater. Med.* (8):227-232 (1997).

22. Mao, C.; Li, H.; Cui, F.; Feng, Q.; Wang, H., Ma, C. Oriented growth of hydroxyapatite on (001) textured titanium with functionalized self-assembled silane monolayer as template. *J. Mater. Chem.* 8(12):2795-2801 (1998).

23. Narayana, K.V.; Venugopal A.; Rama Rao K.S.; Masthan K.; Rao V.V.; Rao P.K. Ammoxidation of 3-picoline over V_2O_5/TiO_2 (anatase) system. II. Characterisation of the catalysts by DTA, SEM, FTIR, ESR and oxygen and ammonia chemisorption. *Applied Catalysis A.: General* (167):11-22 (1997).

24. Nonami, T.; Kamiya, A.; Nagahuma, K.; Kameyama, T. Preparation of hydroxyapatite-granule-implanted superelastic titanium alloy. *J. Meter. Sci. Mater. Med.* (9):203-206 (1998).

25. Quanming, S.; Wang, C.; Weng, S. Electron structure of a grain boundary and a crystal of calcium phosphate bioceramic (hydroxyapatite). *Philosophical Magazine A.* 77(5):1309-1321 (1998).

26. Rhee, S-H. Hydroxyapatite coating on a collagen membrane by a biomimetic method. *J. Am. Ceram. Soc.* 81(11)3029-3031 (1998).

27. Sahay, V.; Lare, P.J.; Hahn, H. Characterization of composite hydroxyapatite (HA) coatings for medical and dental devices. *Characterization and Performance of Calcium Phosphate Coatings for implants, ASTM STP 1196.* Philadelphia. (1994).

28. Sham, T.K.; Lazarus, M.S. X-ray photoelectron spectroscopy (XPS) studies of clean and hydrated TiO_2 (rutile) surface. *Chem. Phys. Lett..* (68):426-432 (1979).

29. Soten, I.; Ozin, G.A. Porous hydroxyapatite-dodecylphosphate composite film on titania-titanium substrate. *J.Mater.Chem.* (9):703-710 (1999).

30. Unnam, J.; Shenoy, R.N.; Clark, R.K. Oxidation of commercial purity titanium. *Oxid. Met.* (23):231-252 (1986).

31. Wang, M.; Yang, X.Y.; Khor, K.A..; Wang Y. Preparation and characterization of bioactive monolayer and functionally graded coatings. *J. Meter. Sci. Mater. Med.* (10):269-273 (1999).

32. Wei, M.; Ruys, A.J.; Swain, M.V.; Kim, S.H.; Milthorpe, B.K.; Sorrell, C.C. Interfacial bond strength of electrophoretically deposited hydroxyapatite coating on metals. *J. Meter. Sci. Mater. Med.* (10):401-409 (1999).

33. Wen, H.B.; Dalmeijer, R.A.J.; Cui, F.Z.; Blitterswijk, C.A.; Groot, K.D. Preparation of calcium phosphate coating on porous tantalum. *J. Mater. Sci. Lett.* (17):925-930 (1998).

34. Weng, W. Sol-gel derived porous hydroxyapatite coating. *J. Meter. Sci. Mater. Med.* (9)159-163 (1998).

35. Zhang, S.; Gonsalves, K.E. Preparation and characterization of thermally stable nanohydroxyapatite. *J. Meter. Sci. Mater. Med.* (8):25-28 (1997).

APPENDICES

APPENDIX A

OXIDE THICKNESS CALCULATION

The equation to calculate the thickness of an oxide layer is given by an exponential equation,

$$Z = 1.5\, t^{1/2} \exp\left(\frac{-27{,}350}{RT}\right) \tag{2}$$

where 27,350 calories/mole is the activation energy for the growth of oxide. T is temperature in degree Kelvin while t is time in seconds, R is the ideal gas constant and Z is oxide thickness in centimeters. This model was derived from oxidation of commercial purity titanium in pure oxygen for temperature no greater than 760 °C (Unnam et al., 1986).

APPENDIX B

HYDROXYAPATITE STRUCTURE

A simplified unit cell of HAP is depicted in Figure B (Kanazawa, 1989) in which oxygen atoms forming the tetrahedra of PO_4 are abbreviated. The two oxygen atoms of the PO_4-tetrahedron are located on the mirror planes at z = 1/4 and 3/4 and the other two occupy symmetrically the sites above and below the planes. Calcium ions occupy two different sites; the column $Ca(Ca_I)$ at z = 0, 1/2 and the screw axis $Ca(Ca_{II})$ at z = 1/4, 3/4. Three of the screw axes Ca^{2+} form a triangle on a mirror plane. A detail of the HAP structure was also explained in Quanming et al. (1998).

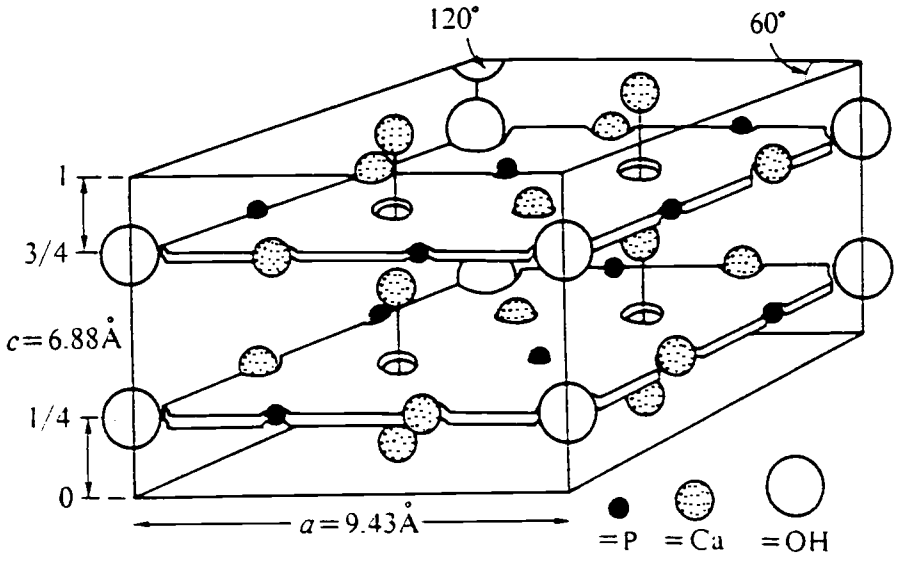

Figure B. Simplified view of an HAP unit cell.

APPENDIX C

UNIT CELLS OF BARE AND HYDROXYLATED TITANIUM

Bullock et al. (1996) showed that the unit cell of bare titanium (without an oxide layer) consists of one six-fold coordinated Ti atom, one five-fold coordinated Ti atom, one two-fold coordinated bridging O atom above the (110) truncated plane, one three-fold coordinated bridging O atom below the plane, and two three-folded coordinated O atoms. The distance between successive (110) planes is 0.325 nm. Its unit cell is shown in Figure C(a). Figure C(b) shows the unit cell of hydroxylated surface. Within this model, approximately half of the five-fold coordinated Ti atoms present at the clean surface become bonded to hydroxyl groups due to water adsorption and dissociation. Similarly, about half of the two-fold coordinated bridging O atoms at the surface become bonded to water-derived hydrogen.

(a) Bare titanium

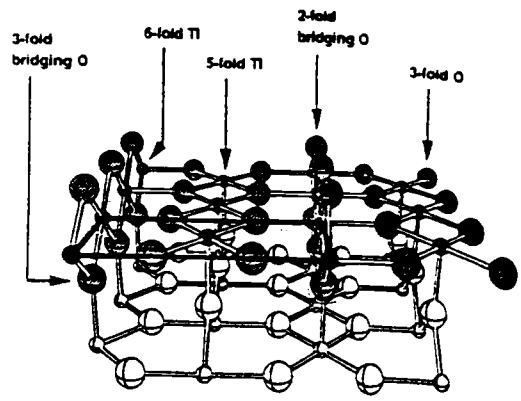

(b) Hydroxylated surface

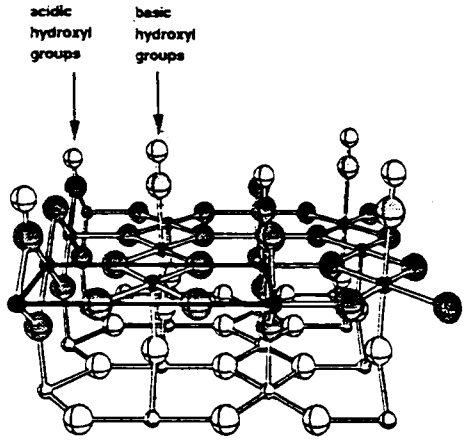

Figure C. Unit cells of (a) bare titanium (without oxide layer) and (b) hydroxylated surface showing acidic and basic hydroxyl groups attached to titanium atoms.

APPENDIX D

EXPERIMENTAL DATA

XPS analysis of different substrates in different solutions is displayed in Table 6. Samples A-K shown are the same as samples A-K in Table 4. Some peaks of each sample are shown in Figure D1-D14. In those figures, the binding energy shown needs to be corrected by adding the amount shown in the last column of Table 6, C 1s binding energy shift (eV), specifically for each sample.

Table 6. XPS analysis of different substrates in different solutions. (samples A-K are the same as samples A-K in Table 4)

Sample	Surface Treatment	Solution Concentration (mM)		Ca/P ratio (sol.)	Conc. Range (only when Ca/P = 1.67)	Aging time (days)	Atomic concentration (%)							Ca/P ratio (surf.)	C 1s binding energy shift (eV)
		P	Ca				P	C	Ca	N	Ti	O	Total		
A	Plain Ti	No immersion in solution			--	--	0	37.9	0	3.7	13.1	45.7	100	--	+ 0.7
B	610 °C, 1 hr, O_2	No immersion in solution			--	--	0	33.4	0	0	11.4	55.3	100	--	+ 0.9
C	610 °C, 1 hr, Air	No immersion in solution			--	--	0	34.8	0	0	11.7	53.6	100	--	+ 0.8
D	610 °C, 1 hr, O_2	1.20	2.00	1.67	Low conc.	10	12.7	12.2	21.1	0	0	54.5	100	1.66	+ 5.9
E	610 °C, 1 hr, O_2	5.45	9.10	1.67	Interm. Conc.	10	0	20.3	3.7	0	16.1	59.9	100	--	+ 0.8
F	610 °C, 1 hr, O_2	12.43	20.73	1.67	High conc.	10	2.9	15.5	3.1	0	23.1	55.8	100	1.07	+ 2.9
G	610 °C, 1 hr, O_2	1.20	2.00	1.67	Low conc.	0.5 (12 hrs)	13.0	14.1	18.2	0	0	54.7	100	1.41	+ 3.7
H	610 °C, 1 hr, O_2	1.20	2.00	1.67	Low conc.	2	10.9	13.6	17.8	0	0	57.7	100	1.62	+ 4.1
I	610 °C, 1 hr, O_2	1.20	2.00	1.67	Low conc.	5	12.2	11.8	19.9	0	0	56.1	100	1.63	+ 5.3
J	Plain Ti	1.20	2.00	1.67	Low conc.	10	2.3	33.6	2.1	3.8	17.7	40.5	100	0.92	+ 1.0
K	610 °C, 1 hr, Air	1.20	2.00	1.67	Low conc.	10	14.4	16.0	18.5	0	0	51.1	100	1.29	+ 4.7
L	610 °C, 1 hr, O_2	0.16	7.60	0.02	--	10	4.2	25.3	0	1.9	13.8	54.9	100	0	+ 0.8
M	800 °C, 10 mins, O_2	0.16	7.60	0.02	--	10	3.6	23.4	0	0	14.2	58.9	100	0	+ 0.7
N	610 °C, 1 hr, O_2	3.70	7.60	0.5	--	10	0	24.6	3.2	0	11.6	60.7	100	--	+ 1.0
O	610 °C, 1 hr, O_2	7.60	7.60	1.0	--	10	3.4	21.5	3.3	0	10.1	61.8	100	0.96	+ 5.3
P	800 °C, 10 mins, Air	1.20	2.00	1.67	Low conc.	10	0	21.2	0	0	10.3	68.5	100	0	+ 0.2
Q	900 °C, 10 mins, Air	1.20	2.00	1.67	Low conc.	10	0	34.5	0	0	16.5	49.0	100	0	+ 0.2

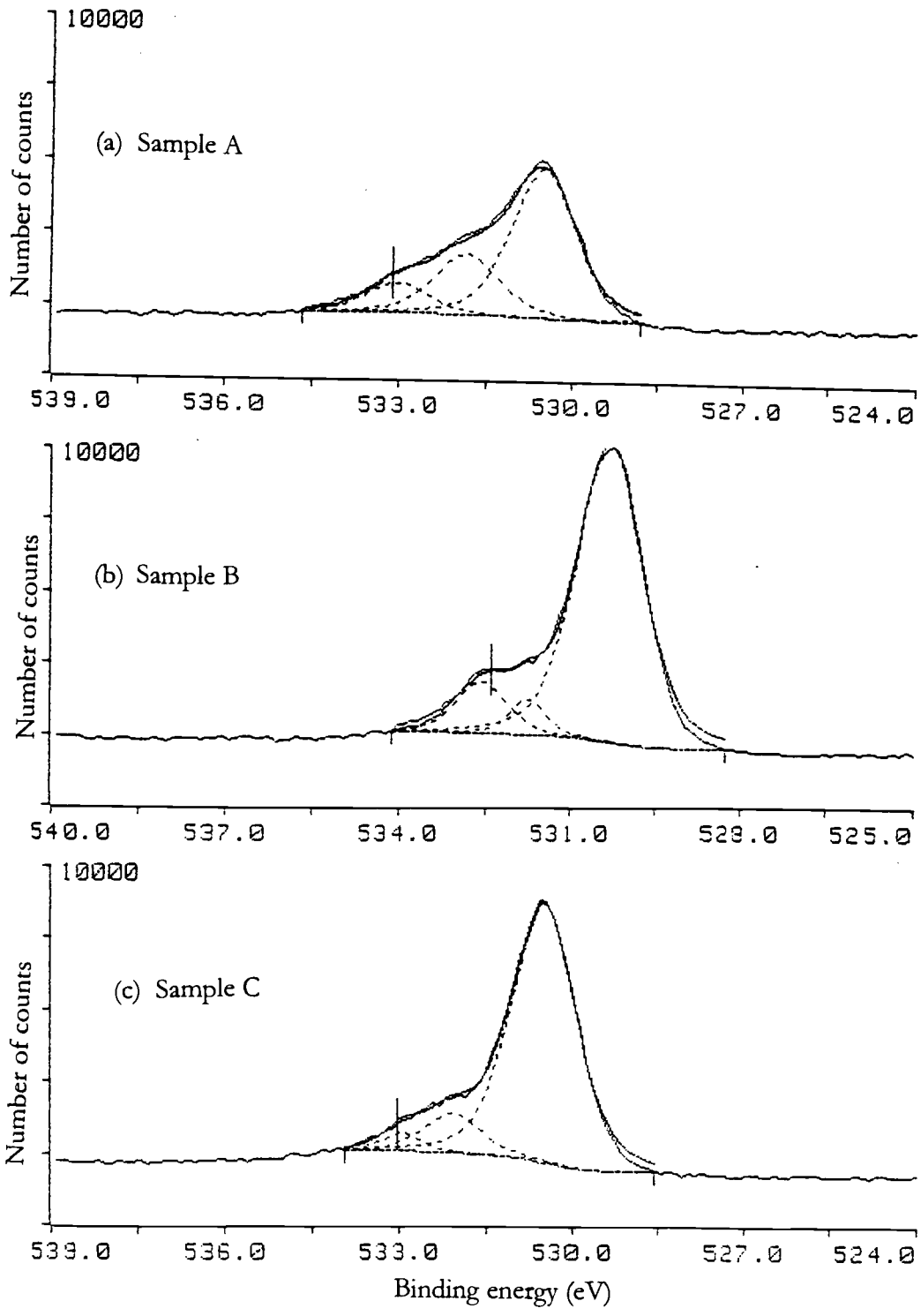

Figure D1. Spectra of O 1s peaks (a) sample A; (b) sample B and (c) sample C.

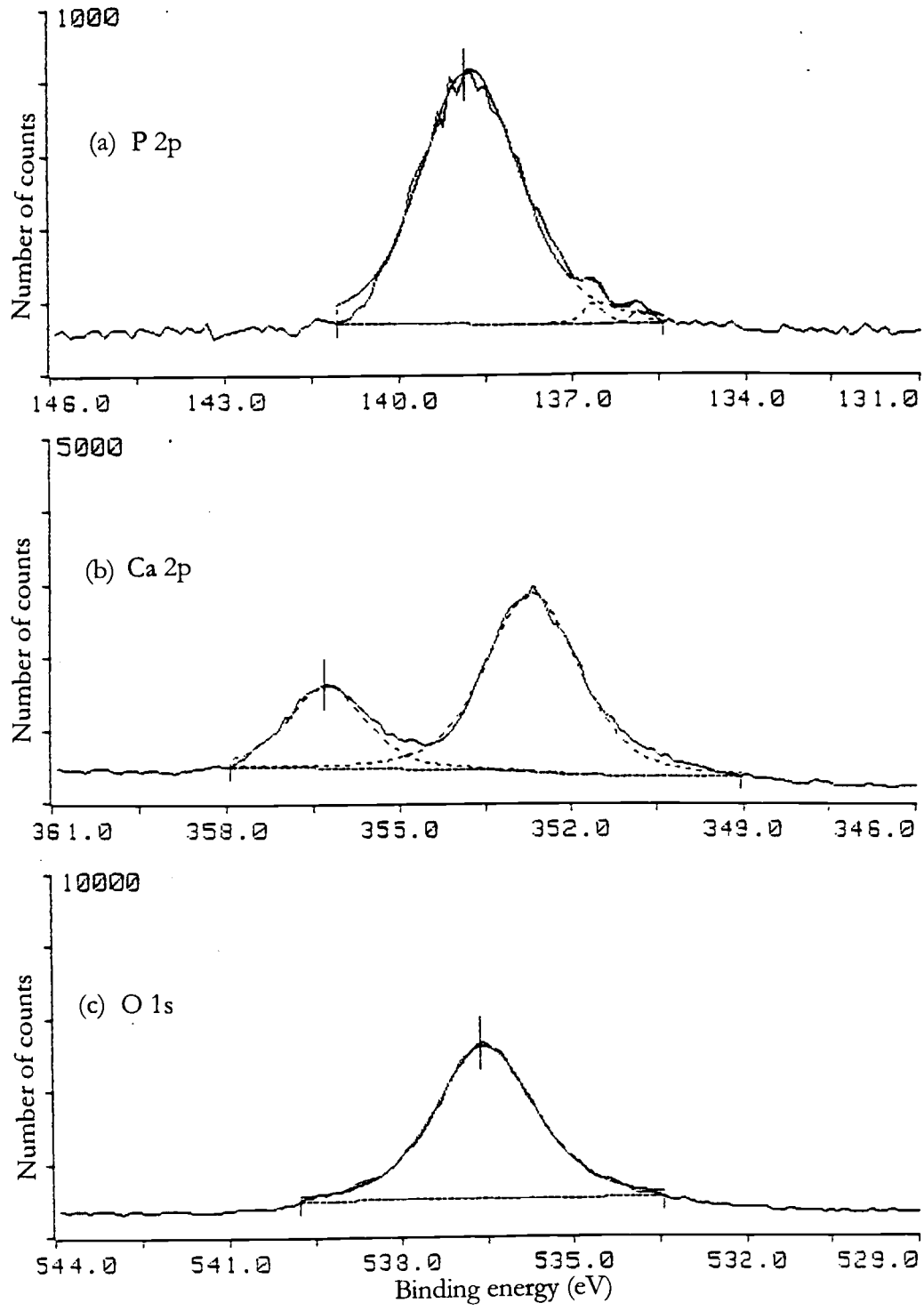

Figure D2. Spectra from sample D for (a) P 2p peaks; (b) Ca 2p peaks and (c) O 1s peak.

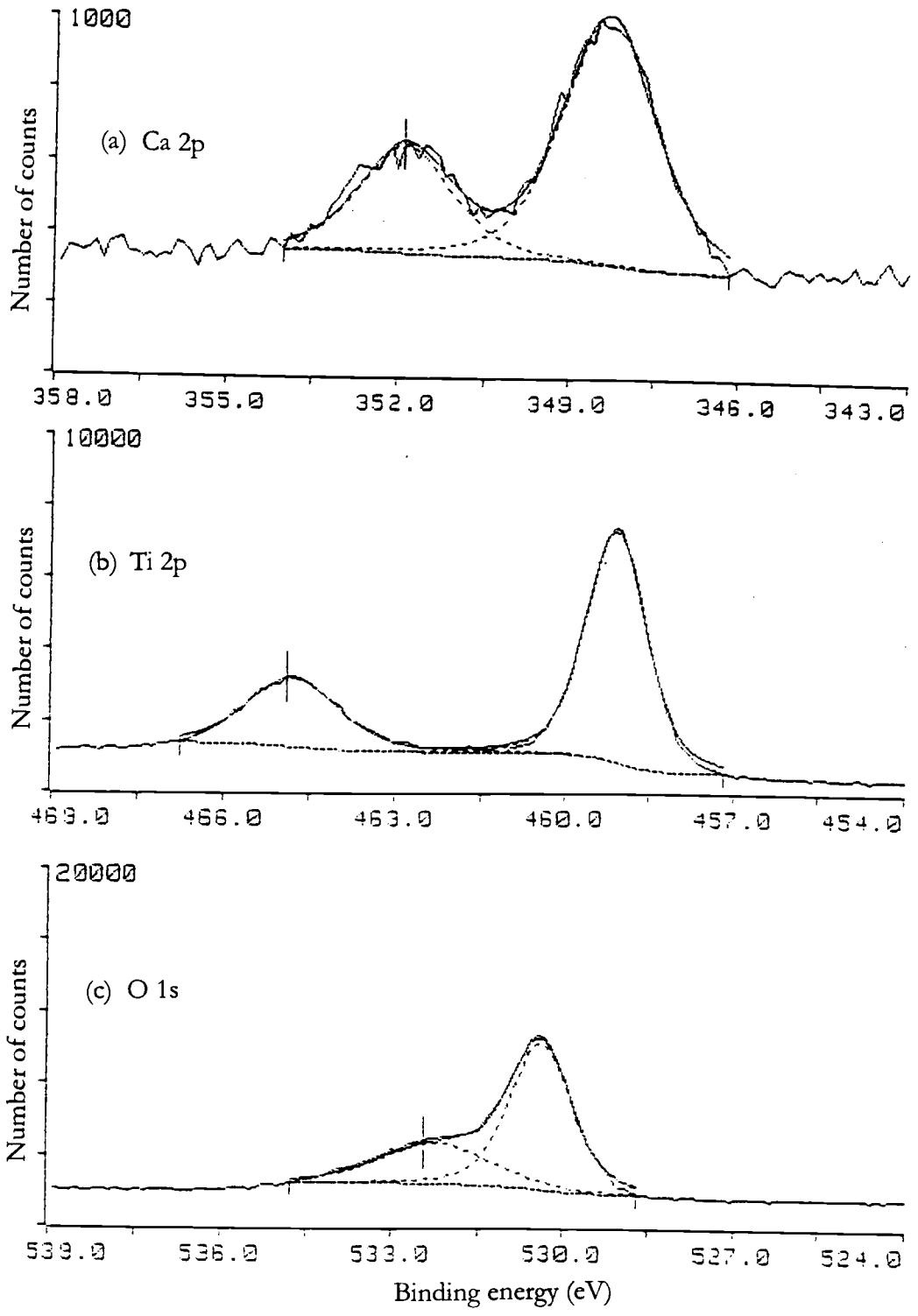

Figure D3. Spectra from sample E for (a) Ca 2p peaks; (b) Ti 2p peaks and (c) O 1s peaks.

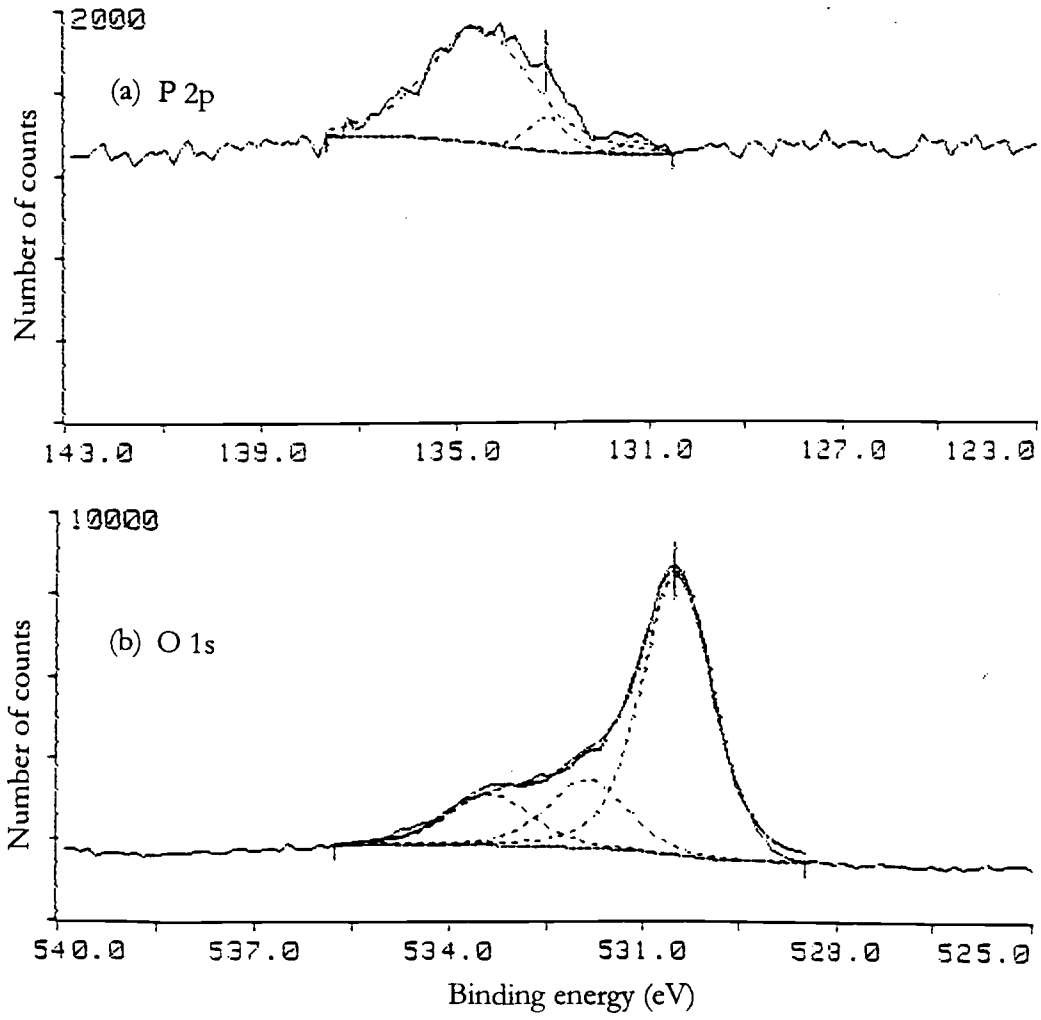

Figure D4. Spectra from sample F for (a) P 2p peaks and (b) O 1s peaks.

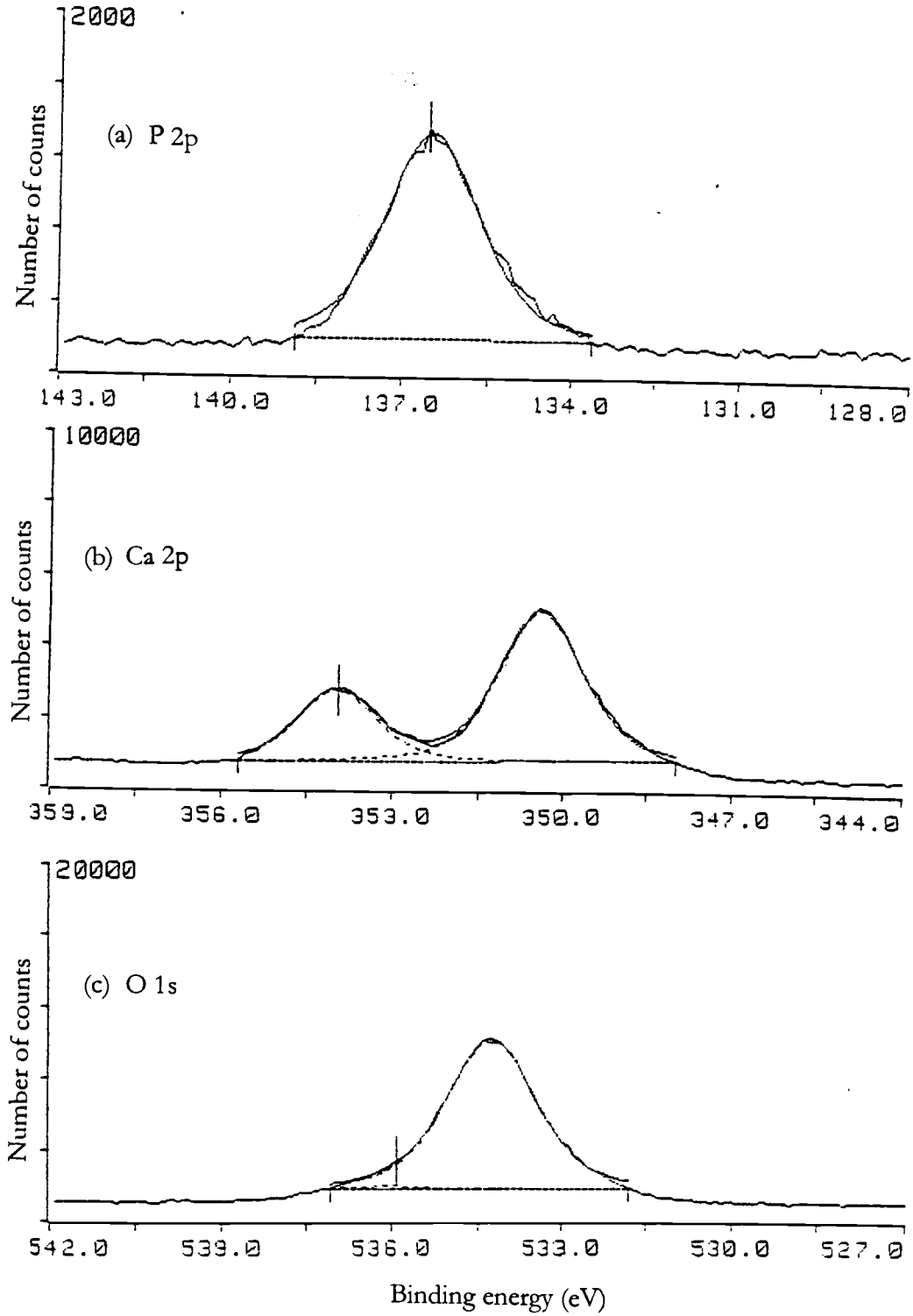

Figure D5. Spectra from sample G for (a) P 2p peak; (b) Ca 2p peaks and (c) O 1s peaks.

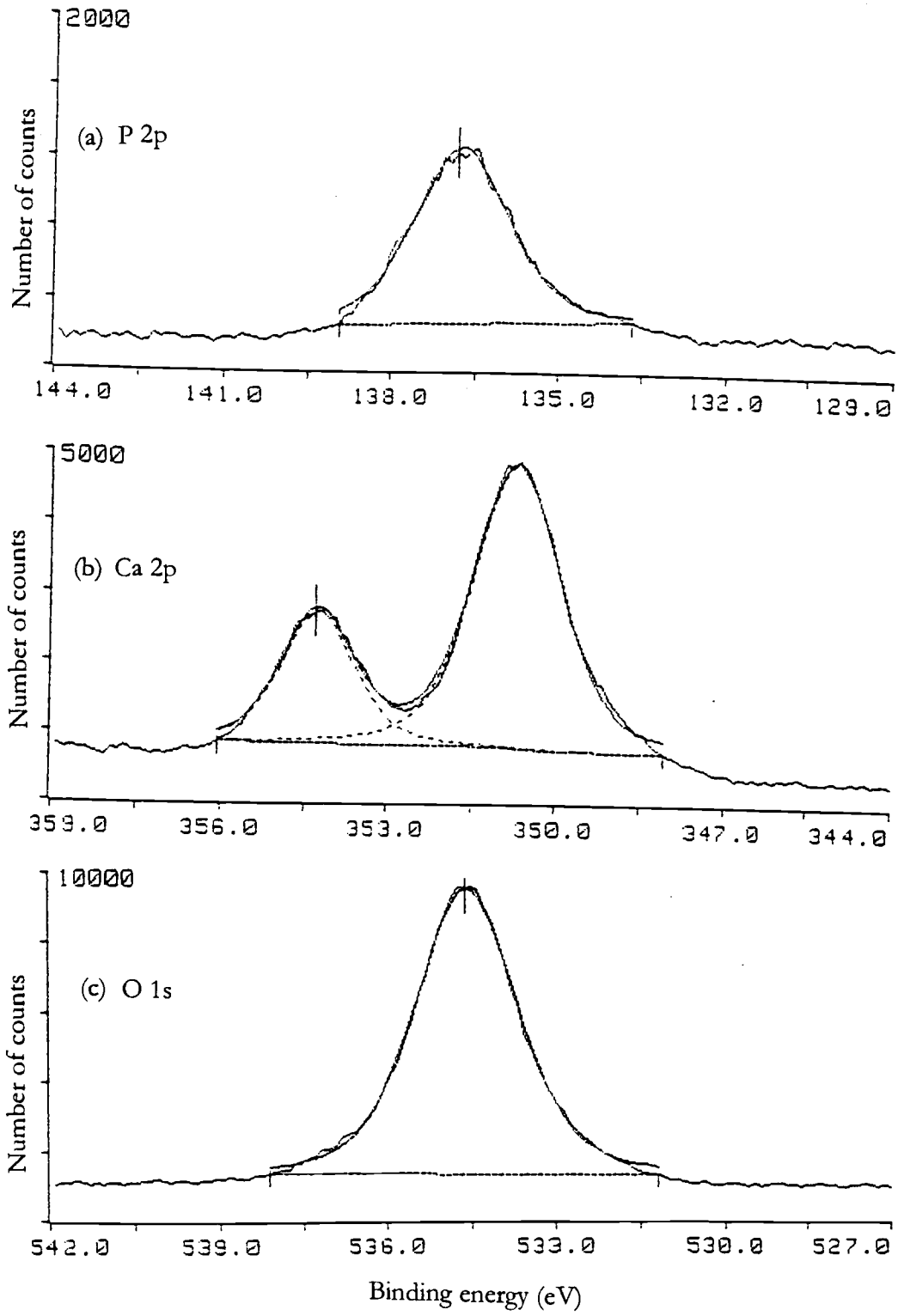

Figure D6. Spectra from sample H for (a) P 2p peak; (b) Ca 2p peaks and (c) O 1s peak.

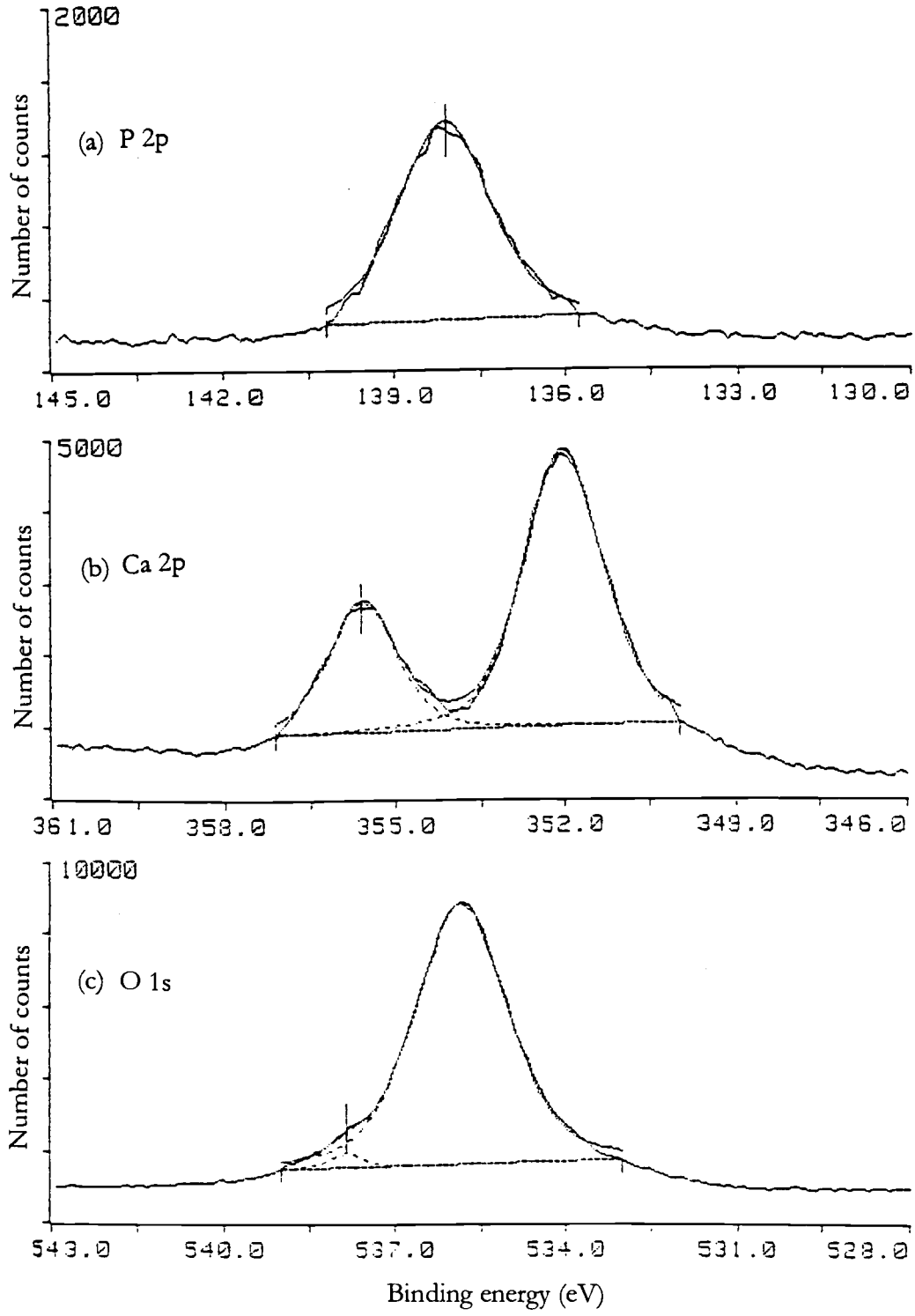

Figure D7. Spectra from sample I for (a) P 2p peak; (b) Ca 2p peaks and (c) O 1s peaks.

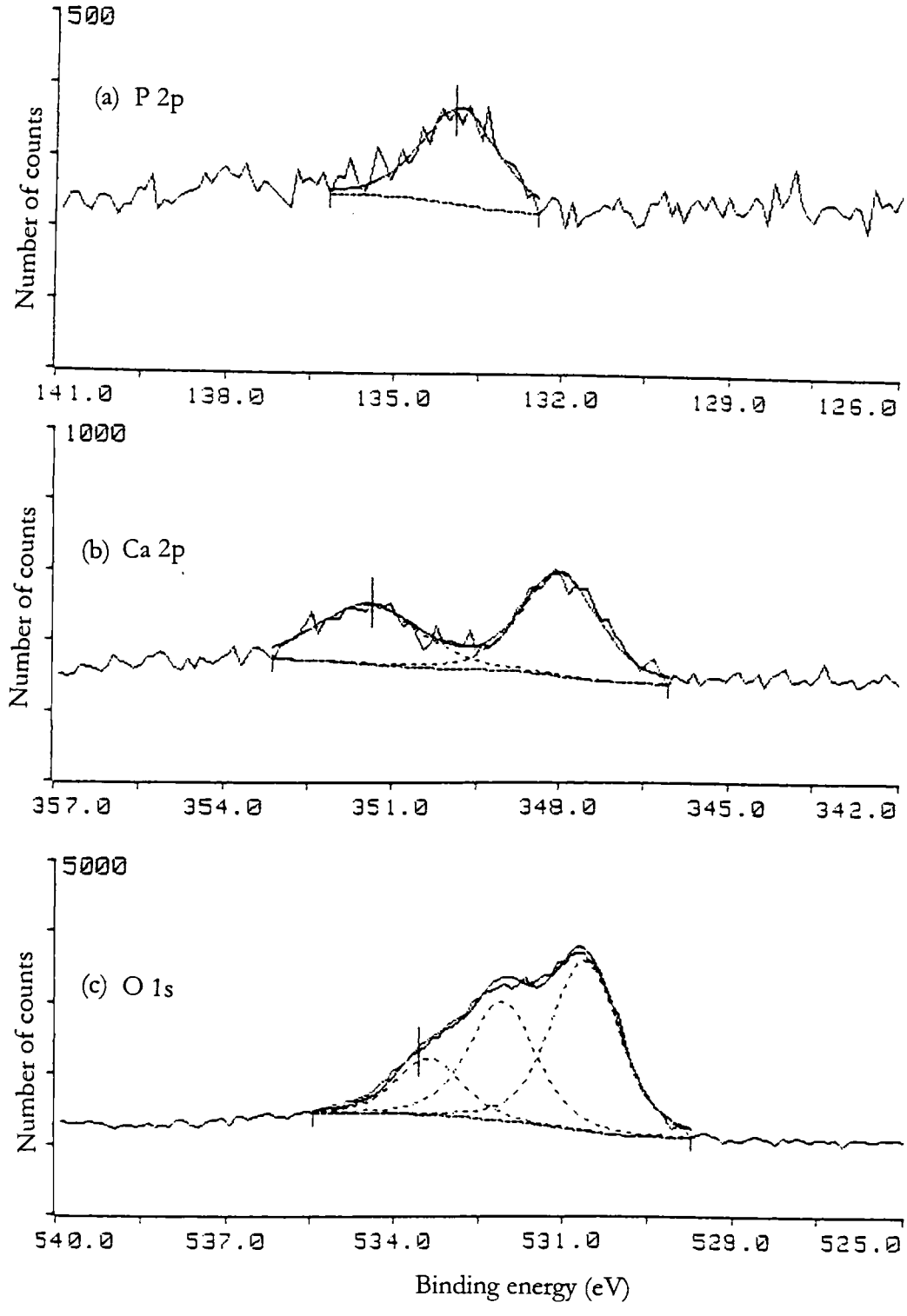

Figure D8. Spectra from sample J for (a) P 2p peak; (b) Ca 2p peaks and (c) O 1s peaks

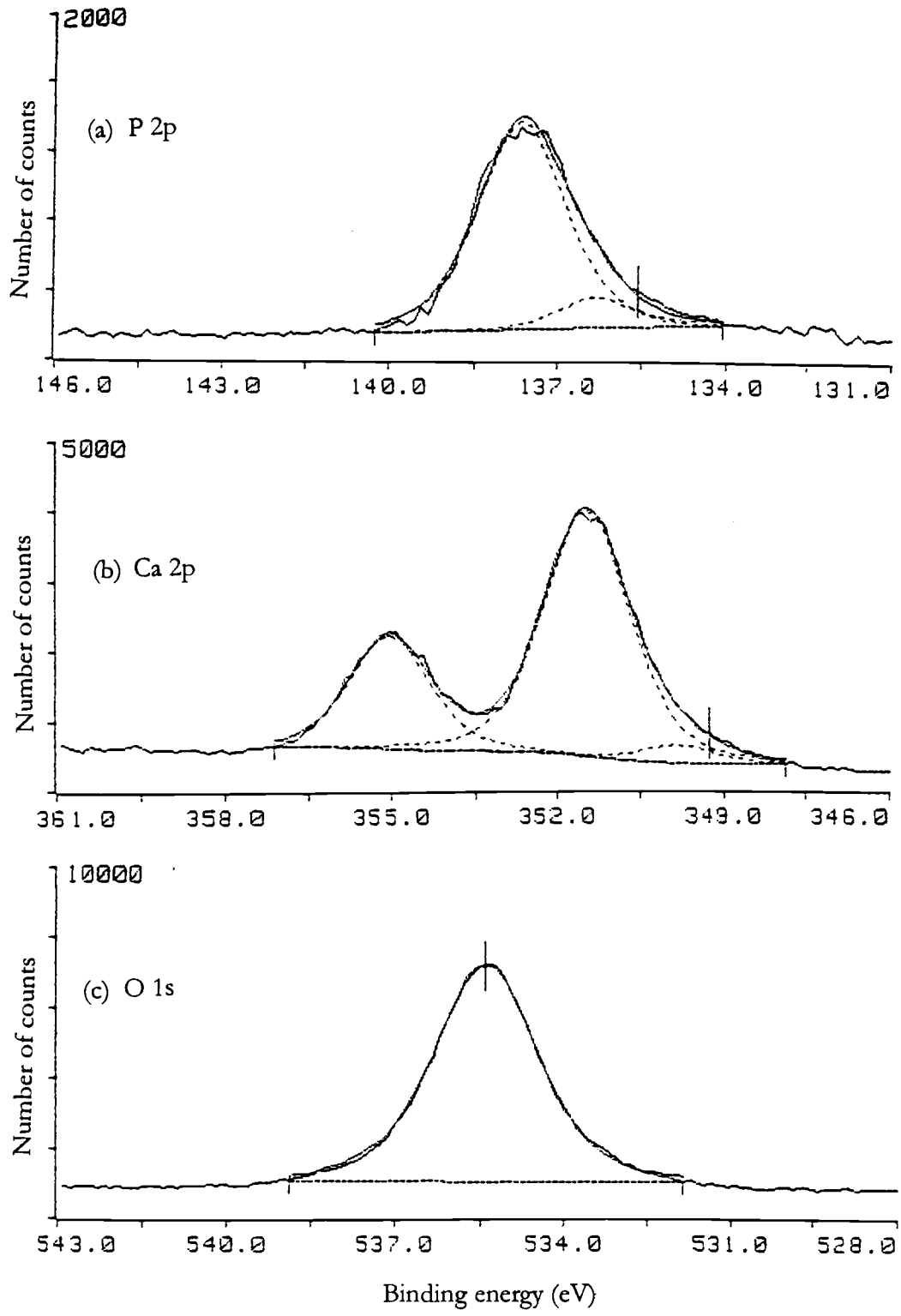

Figure D9. Spectra from sample K for (a) P 2p peaks; (b) Ca 2p peaks and (c) O 1s peak.

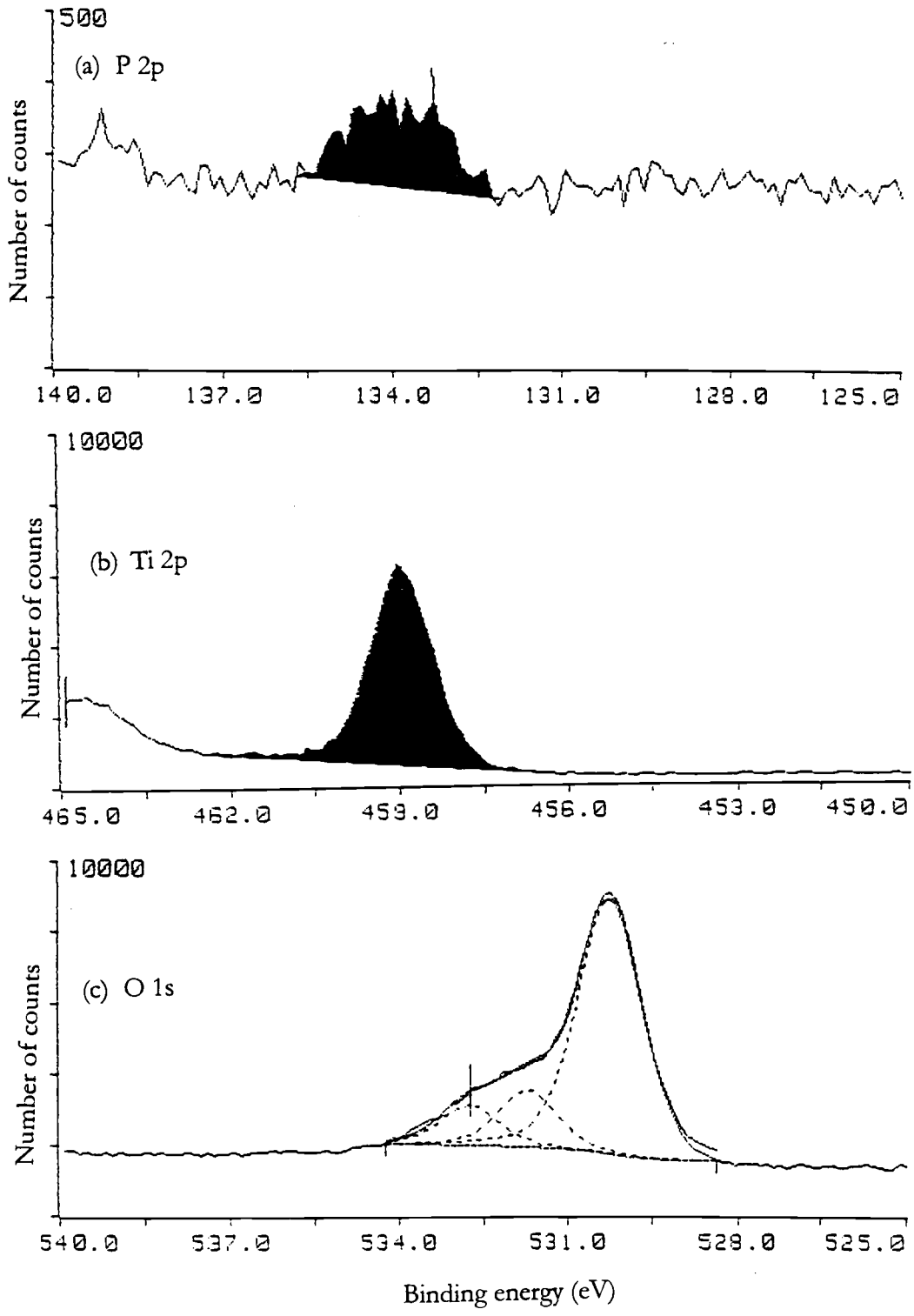

Figure D10. Spectra from sample L for (a) P 2p peak; (b) Ti 2p peak and (c) O 1s peaks.

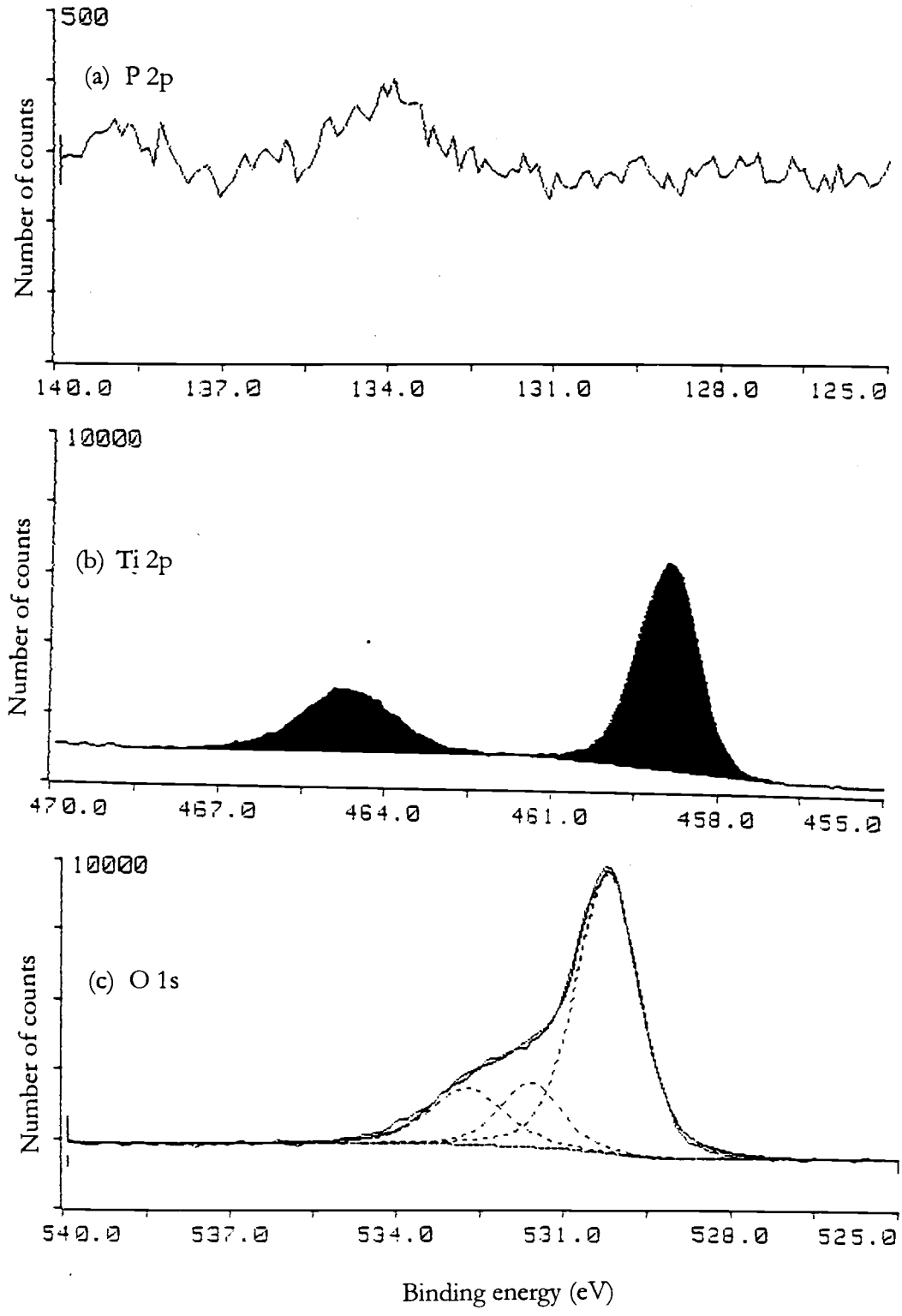

Figure D11. Spectra from sample M for (a) P 2p peaks; (b) Ti 2p peaks and (c) O 1s peaks.

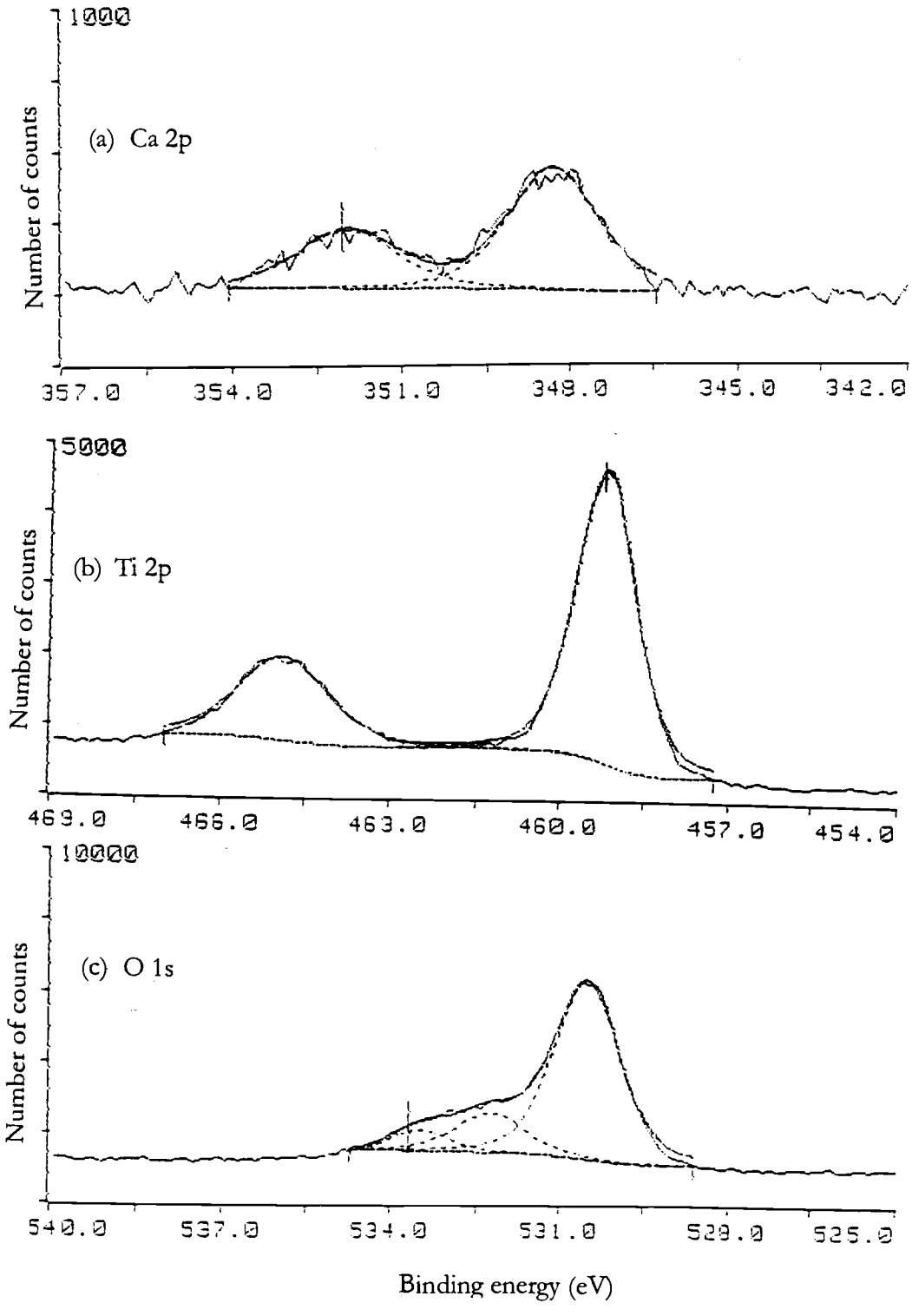

Figure D12. Spectra from sample N for (a) Ca 2p peaks; (b) Ti 2p peaks and (c) O 1s peaks.

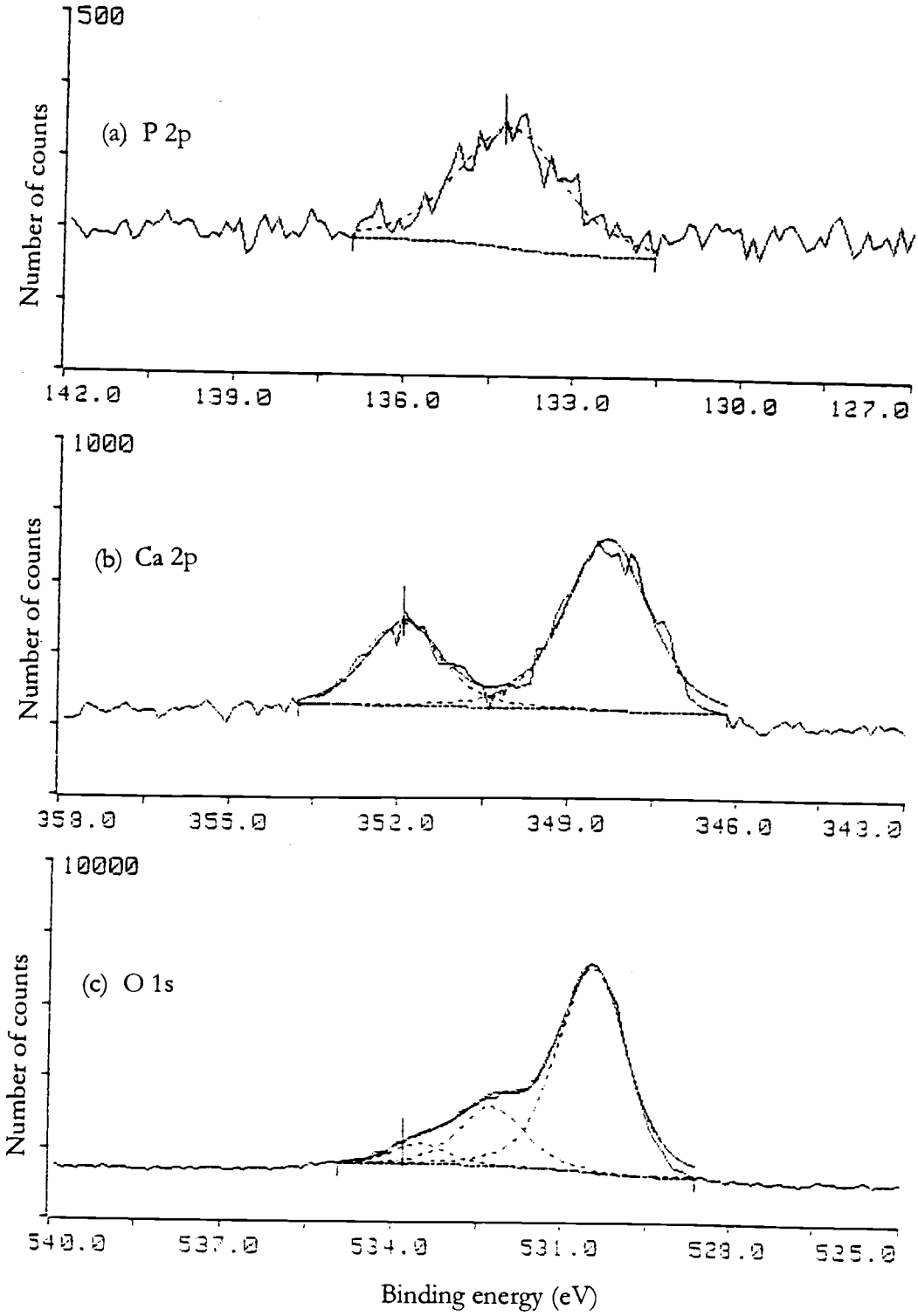

Figure D13. Spectra from sample O for (a) P 2p peak; (b) Ca 2p peaks and (c) O 1s peaks.

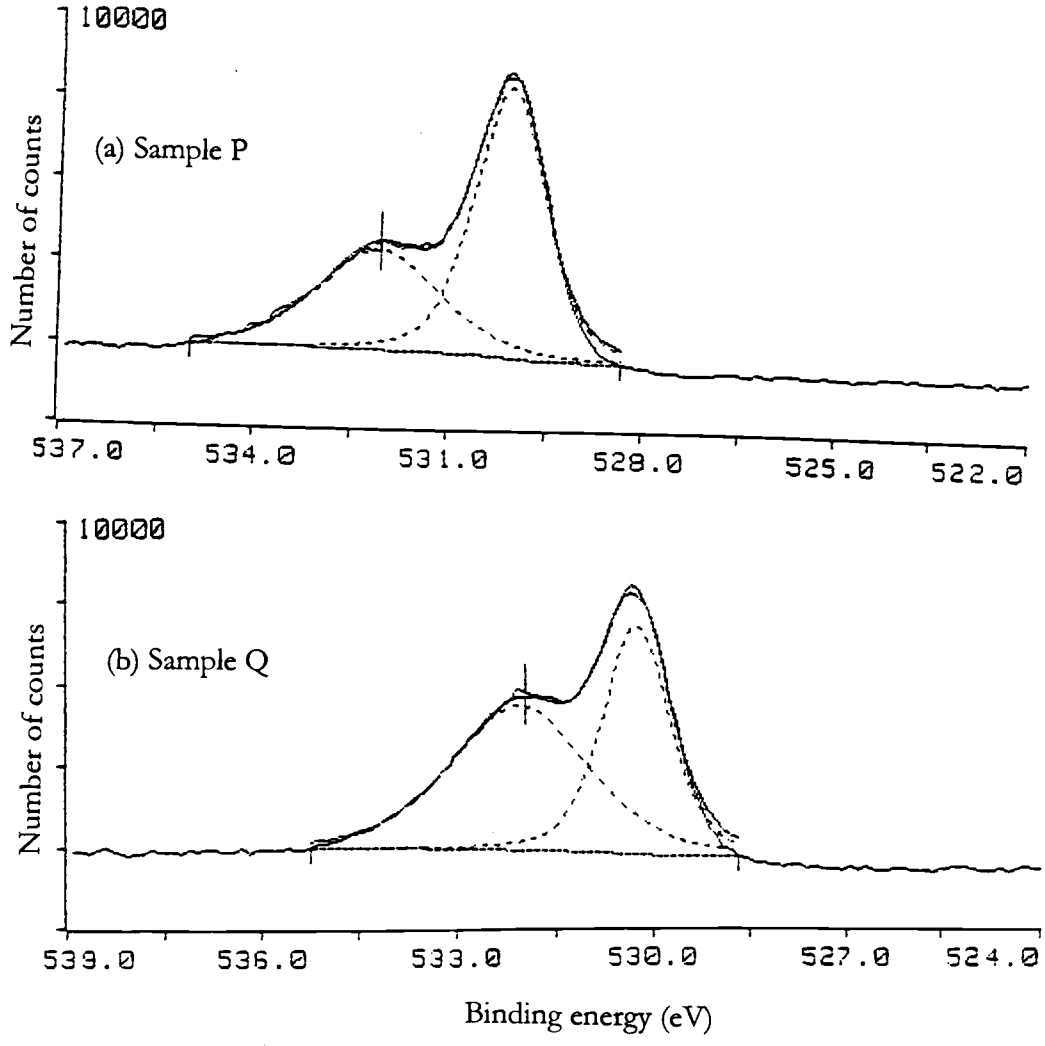

Figure D14. Spectra of O 1s peaks (a) sample P and (b) sample Q.